



UPM
UNIVERSITI PUTRA MALAYSIA
BERILMU BERBAKTI

**A CODED APERTURE-BASED 3D SPECT IMAGING
SYSTEM FOR EARLY BREAST CANCER DETECTION**

By

KHALID HUSSAIN

**Thesis Submitted to the School of Graduate Studies, Universiti Putra Malaysia, in
Fulfilment of the Requirements for the Degree of Doctor of Philosophy**

March 2023

FK 2023 7

All material contained within the thesis, including without limitation text, logos, icons, photographs, and all other artwork, is copyright material of Universiti Putra Malaysia unless otherwise stated. Use may be made of any material contained within the thesis for non-commercial purposes from the copyright holder. Commercial use of material may only be made with the express, prior, written permission of Universiti Putra Malaysia.

Copyright © Universiti Putra Malaysia



DEDICATION

This thesis is gratefully dedicated to:

My beloved mother for her love, patience and understanding.

&

My beloved wife, daughters, son, brothers, and sisters.



Abstract of thesis presented to the Senate of Universiti Putra Malaysia in fulfilment of the requirement for the degree of Doctor of Philosophy

**A CODED APERTURE-BASED 3D SPECT IMAGING
SYSTEM FOR EARLY BREAST CANCER DETECTION**

By

KHALID HUSSAIN

March 2023

Chair : Professor Ts. M. Iqbal bin Saripan, PhD
Faculty : Engineering

Single Photon Emission Computed Tomography (SPECT) is an established imaging modality that is undertaken using a parallel-hole collimator. This technique suffers from clinical limitations as it has less reliability in detecting small lesions (less than one centimeter in diameter) due to trade-off between sensitivity and resolution.

Instead of a collimator, this study proposes a coded aperture (CA) based SPECT imaging system where a mask is attached to a typical clinical gamma camera. This imaging method investigates different patterns of the Modified Uniformly Redundant Array (MURA) masks and mosaic MURA masks by a simulating point source, planar source, and the 3D realistic anthropomorphic female breast phantom. For the breast phantom, simulations were repeated for different lesion sizes and the tumor-to-background ratio (TBR).

The proposed CA-based SPECT camera employs a mosaic MURA mask and antimask combined with the Maximum Likelihood Expectation Maximization (MLEM) algorithm. The antimask reconstructed images are subtracted from the mask images to suppress the background noise and minimize the non-uniformity in the background slice by slice. The reconstructed slices are stacked to give a 3D image. Mosaic MURA mask antimask subtraction has improved the quality of reconstructed images, allowing visualization of 3 mm diameter breast lesions using 10:1 TBR.

The purpose of this research is to prove the feasibility of 3D reconstruction, and the aforementioned background could be shielded either through proper physical shielding and/or through the particular detection angle of a gamma camera. Ultimately, this study has proved that 3D reconstruction of the breast phantom is possible using CA-based SPECT imaging. Moreover, 3D reconstruction can be achieved from a single projection instead of a sinogram. This study has successfully detected a lesion of 3 mm diameter with TBR 10:1. The chest, heart, and lung background radiation effects are not included in this study and can be investigated in future.

Abstrak tesis yang dikemukakan kepada Senat Universiti Putra Malaysia sebagai memenuhi keperluan untuk ijazah Doktor Falsafah

SISTEM PENGIMEJAN SPECT 3D BERASASKAN APERTUR BERKOD UNTUK PENGESANAN AWAL KANSER PAYUDARA

Oleh

KHALID HUSSAIN

March 2023

Pengerusi : Profesor Ts. M. Iqbal bin Saripan, PhD
Fakulti : Kejuruteraan

Pengimejan Komputer Tomografi Pelepasan Foton Tunggal (SPECT) adalah salah satu kaedah yang diterimapakai yang dijalankan menggunakan kolimator lubang selari. Teknik ini mempunyai pengehadan klinikal kerana kurangnya kebolehpercayaan dalam mengesan imej lesion kecil (iaitu untuk diameter kurang daripada satu sentimeter) disebabkan oleh pertukaran antara sensitiviti dan resolusi.

Sebagai ganti kepada kolimator, kajian ini telah mencadangkan sistem pengimejan SPECT berasaskan Apertur Berkod (CA) di mana topeng dipasang pada kamera gamma klinikal. Kaedah pengimejan ini mengkaji corak-corak yang berbeza pada topeng Tatasusunan Lewah Seragam Terubahsuai (MURA) dan topeng MURA mozek dengan mensimulasikan sumber titik, sumber planar, dan antropomorfik realistik 3D fantom payudara wanita. Untuk fantom payudara, simulasi tersebut diulang untuk saiz lesion dan nisbah tumor berbanding latar belakang (TBR) yang berbeza.

Kamera SPECT berasaskan CA yang dicadangkan ini menggabungkan topeng MURA mozek dan antitopeng mozek dengan algoritma Pemaksimuman Jangkaan Kebolehjadian Maksimum (MLEM). Imej-imej antitopeng yang dibina semula ditolak daripada imej topeng untuk menyekat hingar dan meminimumkan ketidakseragaman pada latar belakang, secara berperingkat. Kepingan berperingkat yang dibina semula akan disusun untuk membentuk imej 3D. Penolakan antitopeng daripada topeng MURA mozek telah meningkatkan kualiti imej yang dihasilkan, membolehkan visualisasi lesion payudara berdiameter 3 mm dengan menggunakan TBR pada nisbah 10:1.

Tujuan penyelidikan ini adalah untuk membuktikan kebolehlaksanaan pembinaan semula 3D, dan latar belakang yang disebutkan di atas boleh dilindungi sama ada melalui perisai fizikal yang sesuai dan/atau melalui sudut pengesanan tertentu kamera gamma. Akhirnya, kajian ini telah membuktikan bahawa pembinaan semula 3D fantom payudara

adalah boleh dicapai dengan menggunakan pengimejan SPECT berasaskan CA. Selain itu, pembinaan semula 3D boleh dicapai daripada satu unjuran dan bukannya sinogram. Kajian ini telah berjaya mengesan lesion berdiameter 3 mm dengan nisbah TBR 10:1. Latar belakang kesan sinaran untuk bahagian dada, jantung dan paru-paru tidak termasuk dalam kajian ini dan boleh dikaji pada masa hadapan.



ACKNOWLEDGEMENTS

All praises and thanks to All-Mighty “Allah,” the most merciful, the most gracious, the source of knowledge and wisdom endowed to mankind, who conferred me with the power of mind and capability to take this research thesis to the exciting ocean of knowledge. All respect is for my most beloved Holy Prophet, “Hazrat Muhammad (Peace Be Upon Him),” who is forever a torch of guidance for humanity.

I wish to express my sincere appreciation to my supervisor, Prof. Ts. Dr. M Iqbal Saripan, for the continuous support, expert guidance, motivation, encouragement, and patience throughout the progress of this research. He always helped me and encouraged me to solve the challenges in the way of this research. Besides this, I am also very grateful to my supervisory committee members, Prof. Rozi Mahmud, Dr. Wan Azizun Wan Adnan, and Dr. Mohammed Ali Alnafea, for their expert opinions and valuable support all the time during this research period. I sincerely express my heartiest gratitude Dr. Djeloul Mahboub for his friendly guidance and sincere help during the tough time of the research. I also thank Dr. Dong Xianling for supporting me in developing MCNP Monte Carlo simulations and MATLAB codes for the initial SPECT study.

I want to express my gratitude to Higher Education Commission, Pakistan, for providing the financial support to pursue my Ph.D. study.

I would also like to thank my respected mother, brothers, wife, daughters, and son for always supporting me during this research. They always give me the courage all the way through, spiritually supporting me throughout my life and constantly encouraging me to pursue higher education.

Khalid Hussain
March 2023

This thesis was submitted to the Senate of Universiti Putra Malaysia and accepted as a fulfilment of the requirements for the degree of Doctor of Philosophy. The Members of the Supervisory Committee were as follows:

M. Iqbal bin Saripan, PhD

Professor Ts.
Faculty of Engineering
Universiti Putra Malaysia
(Chairman)

Rozi binti Mahmud, PhD

Professor
Faculty of Medicine and Health Science
Universiti Putra Malaysia
(Member)

Wan Azizun binti Wan Adnan, PhD

Associate Professor
Faculty of Engineering
Universiti Putra Malaysia
(Member)

Mohammed A. Alnafea, PhD

Associate Professor
Department of Radiologic Sciences,
King Saud University
Saudi Arabia
(Member)

ZALILAH MOHD SHARIFF, PhD

Professor and Dean
School of Graduate Studies
Universiti Putra Malaysia

Date: 10 August 2023

TABLE OF CONTENTS

| | Page |
|--|-------------|
| ABSTRACT | i |
| ABSTRAK | ii |
| ACKNOWLEDGEMENTS | iv |
| APPROVAL | v |
| DECLARATION | vii |
| LIST OF TABLES | xii |
| LIST OF FIGURES | xiii |
| LIST OF ABBREVIATIONS | xxi |
| CHAPTER | |
| 1 INTRODUCTION | 1 |
| 1.1 Background | 1 |
| 1.1.1 Breast Cancer | 1 |
| 1.1.2 Detection and Recognition | 1 |
| 1.1.3 Breast Cancer Imaging Modalities | 2 |
| 1.2 SPECT Imaging Modality | 6 |
| 1.3 Problem Statement | 6 |
| 1.4 Research Aims and Objectives | 8 |
| 1.5 Scope and Limitation | 8 |
| 1.6 Thesis Contribution | 9 |
| 2 LITERATURE REVIEW | 11 |
| 2.1 Medical Imaging | 11 |
| 2.2 Radiopharmaceuticals | 12 |
| 2.3 SPECT Imaging | 13 |
| 2.4 Gamma Camera | 15 |
| 2.4.1 Collimator | 15 |
| 2.4.2 Scintillation Detector | 20 |
| 2.4.3 Photomultiplier Tubes | 21 |
| 2.4.4 Signal Analysis and Processing | 22 |
| 2.5 Coded Aperture Imaging Theory | 23 |
| 2.5.1 Research Background | 23 |
| 2.5.2 Coded Aperture Imaging History | 26 |
| 2.5.3 Coded Aperture Image Formation | 31 |
| 2.5.4 Geometric Parameters of Coded Aperture | 32 |
| 2.5.5 Mask and Detector Configuration | 35 |
| 2.5.6 Coded Aperture Patterns | 37 |
| 2.5.7 Near-field Artifacts in Coded Aperture Imaging | 39 |
| 2.6 Monte Carlo Simulation | 40 |
| 2.6.1 Cross Sections | 41 |
| 2.6.2 Photon Interactions | 43 |
| 2.6.3 GATE Monte Carlo Simulation | 47 |
| 2.6.4 MCNP5 Monte Carlo Simulation | 49 |
| 2.7 Reconstruction Methods | 50 |
| 2.7.1 Correlation Techniques | 50 |

| | | |
|----------|--|-----------|
| 2.7.2 | Filtered Back Projection | 50 |
| 2.7.3 | Iterative Reconstruction | 51 |
| 2.8 | Summary | 52 |
| 3 | MATERIALS AND METHODS | 53 |
| 3.1 | Design of SPECT Camera in Simulation Environment | 54 |
| 3.1.1 | Geometrical Structure of SPECT Camera | 55 |
| 3.1.2 | Point Source Simulation Using MCNP5 | 55 |
| 3.1.3 | Point Source Simulation Using GATE\ | 56 |
| 3.1.4 | Energy Windowing and Blurring Process | 57 |
| 3.1.5 | Model Validation | 57 |
| 3.2 | Near Field Coded Aperture Imaging | 60 |
| 3.3 | General simulation setup | 61 |
| 3.4 | Point Source Imaging Using MURA Mask | 63 |
| 3.4.1 | Point Source Simulation Setup | 63 |
| 3.4.2 | Two Point Sources | 64 |
| 3.4.3 | Planar Source | 65 |
| 3.4.4 | Near-field Correction | 66 |
| 3.5 | Design of SPECT Model for 3D Breast Imaging | 66 |
| 3.5.1 | Geometrical Structure | 66 |
| 3.5.2 | Modelling of Anthropomorphic Breast Phantom | 69 |
| 3.5.3 | Voxelized Breast Source Modelling | 72 |
| 3.5.4 | Anthropomorphic Breast Phantom Activity | 73 |
| 3.5.5 | Mosaic MURA Mask | 73 |
| 3.5.6 | Simulating the Breast Phantom | 76 |
| 3.5.7 | Image Reconstruction | 76 |
| 3.5.8 | Performance Evaluation | 78 |
| 3.6 | Summary | 79 |
| 4 | RESULTS AND DISCUSSION | 80 |
| 4.1 | Validation of the Simulated SPECT model | 80 |
| 4.1.1 | Intrinsic Spatial Resolution | 80 |
| 4.1.2 | Intrinsic energy resolution | 82 |
| 4.1.3 | System Spatial Resolution and Sensitivity | 82 |
| 4.2 | Coded Aperture imaging performance analysis | 84 |
| 4.2.1 | Ideal Point Source | 85 |
| 4.2.2 | Point Source Simulation Results using MURA Mask | 85 |
| 4.2.3 | Two Point Sources | 87 |
| 4.2.4 | Point Source Simulation Results using Mosaic MURA Mask | 90 |
| 4.2.5 | Near-field Correction | 91 |
| 4.2.6 | Planer source simulation results using MURA mask | 92 |
| 4.3 | Evaluating Beast Phantom Images | 94 |
| 4.3.1 | MURA Imaging Assessment | 95 |
| 4.3.2 | Mosaic MURA Imaging Assessment | 102 |
| 4.3.3 | Results Comparison of MURA vs. mosaic MURA mask | 115 |
| 4.3.4 | Results analysis | 119 |
| 4.4 | Performance Analysis | 119 |
| 4.5 | Summary | 120 |

| | | |
|----------|-----------------------------|-----|
| 5 | CONCLUSION | 121 |
| 5.1 | Summary | 121 |
| 5.2 | Future work | 122 |
| | REFERENCES | 123 |
| | APPENDICES | 140 |
| | BIODATA OF STUDENT | 141 |
| | LIST OF PUBLICATIONS | 142 |



LIST OF TABLES

| Table | | Page |
|-------|---|------|
| 2.1 | Factors that affect the parallel-hole collimator performance | 19 |
| 2.2 | Specifications and functionality of many standard commercially available parallel-hole collimators | 20 |
| 2.3 | Some important characteristics of the scintillators crystals that are most often used for SPECT imaging | 21 |
| 3.1 | SIEMENS Symbia T SPECT camera specifications | 56 |
| 3.2 | Main simulation parameters of CA imaging using point source(s) | 64 |
| 3.3 | Breast SPECT simulation parameters | 67 |
| 3.4 | Material composition of all components used in the simulation | 68 |
| 3.5 | Ellipsoidal parameters for breast phantom models | 71 |
| 3.6 | Activity range translation Table for breast phantom materials | 73 |
| 3.7 | Breast and tumor size for simulation | 76 |
| 4.1 | Specifications obtained by simulation and experiment provided by the manufacturer | 84 |
| 4.2 | MURA mask/antimask results of CBR, PSNR, and MSE were measured from a reconstructed breast phantom of lesion sizes of 8 mm, 6 mm, 4 mm, and 3 mm with TBR 10:1 | 102 |
| 4.3 | Mosaic MURA mask/antimask results of CBR, PSNR, and MSE were measured from a reconstructed breast phantom of lesion sizes of 8 mm, 6 mm, 4 mm, and 3 mm with TBR 10:1 | 108 |
| 4.4 | MURA mask results of CBR, PSNR, and MSE were measured from a reconstructed breast phantom of lesion sizes of 8 mm, 6 mm, 4 mm, and 3 mm with TBR 10:1 | 110 |
| 4.5 | Mosaic MURA mask/antimask results of CBR, PSNR, and MSE were measured from a reconstructed breast phantom of lesion sizes of 8 mm, 6 mm, 4 mm, and 3 mm with TBR 5:1 | 112 |

LIST OF FIGURES

| Figure | | Page |
|--------|---|------|
| 1.1 | An overview of breast cancer imaging techniques | 2 |
| 1.2 | MRI has a high resolution, and it can be revealed by comparing (a) mammography screening with (b) MRI screening | 3 |
| 1.3 | Mammography and MRI diagnosis, (a) mammography missed lesion, (b) while the lesion is clearly visible in MRI examination | 4 |
| 1.4 | Gamma camera imaging vs. mammography, (a) left craniocaudal mammogram, (b) right craniocaudal mammogram, (c) left craniocaudal gamma imaging, and (d) right craniocaudal gamma | 5 |
| 2.1 | Block diagram of the literature review | 12 |
| 2.2 | SIEMENS Symbia T SPECT Camera | 14 |
| 2.3 | Schematic diagram of gamma camera showing various components | 15 |
| 2.4 | Various diagrams of collimator used in gamma camera, (a) parallel hole, (b) pin-hole, (c) diverging-hole, and (d) converging hole collimator | 16 |
| 2.5 | Schematic diagram of wire mesh collimator designs, (a) WMC1, (b) WMC2, (c) multihole collimator | 17 |
| 2.6 | Profile of multi-hole collimator. The FWHM is used to measure resolution | 18 |
| 2.7 | Schematic diagram of Scintillation counter consisting of a crystal coupled with a PMT | 21 |
| 2.8 | The basic concept behind a pinhole camera | 25 |
| 2.9 | Multiple pinholes camera based on coded aperture mask | 25 |
| 2.10 | A random array of 41x41 size and its PSF, (a) a mask developed from the random array with 41x41 elements, (b) reconstructed object depicting the noise in random array mask, (c) 3D plot of the random array point spread function, (d) profile of the decoded image. | 27 |
| 2.11 | Non-redundant array and its 3D response function: (a) a non-redundant array binary pattern with 19x19 elements (b) a 3D plot of its point spread function representing the non-ideal imaging characteristics | 28 |

| | | |
|------|---|----|
| 2.12 | The geometric array of L shape binary pattern and the 3D response of its PSF, (a) a binary pattern of 9x9 L shape array elements, yellow corresponds to 1, the open area and blue corresponds to 0, the close area (b) a 3D plot of PSF representing the non-ideal imaging characteristics. | 28 |
| 2.13 | The geometric array of X shape binary pattern and the 3D response of its auto-correlation function, (a) a binary pattern of 9x9 X shape array elements, blue represent 0's and yellow represent 1's, (b) a 3D plot of point spread function representing the non-ideal imaging characteristics. | 29 |
| 2.14 | Binary pattern of URA CA mask and its point spread function: (a) URA binary pattern of 61x59 elements where yellow represents 1's and blue represents 0's, (b) 3D plot of its correlation function. | 30 |
| 2.15 | Binary MURA mask of 101x101 size and its point spread function: (a) a binary MURA mask of 101x101 elements, where yellow represents 1's and blue represents 0's, (b) 3D point spread function of a decoded image showing a perfect point spread function | 30 |
| 2.16 | Binary NTHT mask of 82x82 size and its point spread function: (a) NTHT binary mask developed from basic 41x41 MURA pattern where yellow represents 1's and blue represent 0's, (b) 3D point spread function of a decoded image showing a perfect point spread function | 31 |
| 2.17 | A schematic illustration of point source coded aperture imaging | 32 |
| 2.18 | Fundamental geometry of CA imaging depicting the point of intersection of a ray traveling from r_o to r_i | 33 |
| 2.19 | Geometric parameters of the coded aperture: (a) measuring the magnification factor, (b) measuring the geometric resolution of the mask | 33 |
| 2.20 | A simple geometry representing the imaging FoV | 34 |
| 2.21 | Geometric parameters of coded aperture: (a) linear relationship between geometric resolution and FoV, (b) geometric resolution against magnification factor | 35 |
| 2.22 | The three potential mask camera configurations are as follows: (a) both the camera and mask have the same dimensions, (b) the detector is bigger than the mask, and (c) the mosaic mask of 2x2 of basic pattern, which is bigger than the detector | 36 |
| 2.23 | The MURA CA mask and its response function, (a) the binary pattern of the MURA mask, (b) the 3D response function (PSF) of an ideal (no noise) binary MURA mask correlation. | 38 |

| | | |
|------|---|----|
| 2.24 | Mosaic mask and its 3D PSF, (a) the mosaic MURA binary mask with 82x82 elements, blue color denotes 0's while yellow color denotes 1's, (b) the PSF of the mosaic MURA, it shows additional copies of the source object that may help to increase the image contrast. | 39 |
| 2.25 | Principles of Monte Carlo simulations of an imaging system | 41 |
| 2.26 | Plots of attenuation coefficients for NaI | 42 |
| 2.27 | Particle interaction types flowchart | 44 |
| 2.28 | Comparative significance of two primary forms of X-ray interaction. The line depicts the Z and photon energy levels at which the photoelectric and Compton effects are equal | 45 |
| 2.29 | Diagram of photoelectric effects mechanics explaining the photoelectric effect | 46 |
| 2.30 | An illustration of GATE's layered architecture | 48 |
| 2.31 | The digitizer is structured as a series of modules that start from the hit and end with the single, which represents the physical observable viewed by the detector | 49 |
| 2.32 | Block diagram of the iterative image reconstruction method | 51 |
| 3.1 | The main workflow of the proposed methodology | 54 |
| 3.2 | Geometrical Structure of SPECT Camera developed using MCNP5 | 55 |
| 3.3 | Geometrical Structure of SPECT Camera developed using GATE | 57 |
| 3.4 | Pencil beam source simulation for measuring intrinsic spatial resolution of scintillation camera | 59 |
| 3.5 | A General representation of the coded aperture projection geometry | 61 |
| 3.6 | Attenuation coefficient as a function of mask thickness for lead and tungsten material for incident photons with energy of 140 keV | 62 |
| 3.7 | Schematic GATE Monte Carlo simulation diagram using a point source with 10^8 particles. The MURA CA mask consists of 97x97 elements in near-field imaging geometry | 64 |
| 3.8 | Planar source simulated geometrical structure using GATE | 65 |
| 3.9 | Visualization of geometrical structure for breast phantom simulation using GATE | 67 |

| | | |
|------|---|----|
| 3.10 | An illustration of real breast anatomy | 70 |
| 3.11 | The Anthropomorphic breast phantom with 8 mm diameter tumor | 70 |
| 3.12 | The 3D background mixture of breast phantom, (a) $\alpha = 1$, (b) $\alpha = 2$ | 71 |
| 3.13 | The skin layer (a), and ductal network (b) of the female anthropomorphic breast phantom | 72 |
| 3.14 | The MURA binary mask and PSF of its auto-correlation function, (a) mask patterns of 83x83 elements, in (a) blue color denotes 0's while yellow color denotes 1's, (b) the 3D PSF of the auto-correlation function of mask. | 74 |
| 3.15 | In the mosaic MURA binary mask with 166x166 elements, blue color denotes 0's while yellow color denotes 1's. The basic 83x83 MURA pattern was used to build this mosaic configuration. | 75 |
| 3.16 | The PSF of the mosaic MURA, it shows additional copies of the source object that may help to increase the image contrast | 75 |
| 3.17 | 3D reconstructed breast phantom with 8mm tumor (a) planer view and (b) 3D view | 77 |
| 3.18 | ROI and background region in the planar view of the 3D reconstructed breast phantom with 8mm lesion | 78 |
| 4.1 | Generated image and its profile through the center fitted by Gaussian function using (a) GATE and, (b) MCNP5 | 81 |
| 4.2 | Comparison between the proposed simulated image profile and Guassian function | 81 |
| 4.3 | Energy spectrum with Gaussian function fitted over the data | 82 |
| 4.4 | Generated image of point source and its profile through the center fitted by Gaussian function using (a) GATE and, (b) MCNP5 | 83 |
| 4.5 | Comparison between the simulated point source image profile and Gaussian function | 84 |
| 4.6 | The characteristics of a MURA coded aperture mask have perfect correlation properties. (a) The MURA mask consists of binary patterns of 97 x 97 elements, (b) an ideally decoded image of the point source, i.e., the cross-correlation of the mask (a) with its decoding function G, (c) a 3D plot of an ideal point source decoded image, (d) an ideal image profile through its center | 85 |

| | | |
|------|---|----|
| 4.7 | Monte Carlo simulation of a point source, (a) the raw projection (shadowgram) of the mask on the detector, (b) the decoded image of the point source, i.e., the cross-correlation of the simulated raw projection image, (a) with its decoding function G, (c) decoded image profile through its center | 86 |
| 4.8 | Reconstructed point source image and its profile using MURA CA mask and reconstructed with MLEM iterative reconstruction algorithm | 87 |
| 4.9 | A Monte Carlo simulation of two off-axis point sources (a) the raw projection image of the mask on the detector; (b) the decoded image of two point sources, i.e., the cross-correlation of the simulated raw projection image, point sources' centers are separated by 10 mm distance (a) with its decoding function G; (c) 3D plot of decoded images; and (d) the decoded image profile through its center. | 88 |
| 4.10 | Monte Carlo simulation of two off-axis point sources separated by 1.9mm (a)) decoded image of two point sources, i.e., the cross-correlation of the simulated raw projection image, (b) the decoded image profile through its center, two points are not clearly visible. | 89 |
| 4.11 | Monte Carlo simulation of two off-axis point sources separated by 1.9mm (a) reconstructed image of two point sources using MLEM reconstruction, (b) reconstructed image profile through its center, two points are clearly visibly | 90 |
| 4.12 | Reconstructed point source image and its profile using mosaic MURA CA mask and reconstructed with MLEM algorithm | 91 |
| 4.13 | Projection of the simulated point source (a), corrected projection after near-field correction (b), and the reconstructed image of the point source without correction (c) and with correction (d). | 92 |
| 4.14 | Decoded image of a planar source using correlation method, (a) decoded image, (b) image profile through the center | 93 |
| 4.15 | Reconstructed image of a planar source using MLEM method, (a) decoded image, (b) image profile through the center | 93 |
| 4.16 | Ideal breast slices of 1 mm thickness taken from the different depths of tumor, (a) ideal breast slice at 12.5% depth of tumor, (b) ideal breast slice at 25% depth of tumor, (c) ideal breast slice at 37.5% depth of tumor, (d) ideal breast slice at 50% depth of tumor, (e) ideal breast slice at 62.5% depth of tumor, (f) ideal breast slice at 75% depth of tumor | 96 |

- 4.17 MURA CA reconstructed slices of an 8 mm tumor from 12.5% to 37.5% depth, and each slice has a thickness of 1 mm : (a) reconstructed slice at 12.5% depth of tumor using mask, (b) reconstructed slice at 12.5% depth of tumor using antimask, (c) difference between mask and antimask, (d) breast phantom reconstructed slice at 25% depth of tumor using mask, (e) breast phantom reconstructed slice at 25% depth of tumor using antimask, (f) difference between mask and antimask at 25% depth of tumor, (g) breast phantom reconstructed slice at 37.5% depth of tumor using the mask, (h) breast phantom reconstructed slice at 37.5% depth of tumor using antimask, (i) difference of mask and antimask at 37.5% depth of the tumor. The TBR used is 10:1. 97
- 4.18 MURA CA reconstructed slices of an 8 mm tumor from 50% to 75% depth; each slice has a thickness of 1 mm : (a) reconstructed slice at 50% depth of tumor using mask, (b) reconstructed slice at 50% depth of tumor using antimask, (c) difference of mask and antimask, (d) breast phantom reconstructed slice at 62.5% depth of tumor using mask, (e) breast phantom reconstructed slice at 62.5% depth of tumor using antimask, (f) difference of mask and antimask at 62.5% depth of tumor, (g) breast phantom reconstructed slice at 75% depth of tumor using mask, (h) breast phantom reconstructed slice at 75% depth of tumor using antimask, (i) difference of mask and antimask at 75% depth of the tumor. The TBR used is 10:1. 98
- 4.19 Breast phantom reconstructed images using MURA mask/antimask with (a) 8 mm tumor, (b) 6 mm tumor, (c) 4 mm tumor, and (d) 3 mm tumor. The TBR used is 10:1. 99
- 4.20 Breast phantom vertical profile through the center of tumor using MURA mask/antimask with a diameter of 8 mm (a) and 6 mm (b) 100
- 4.21 Breast phantom vertical profile through the center of tumor using MURA mask/antimask with a diameter of 4 mm (a) and 3 mm (b) 101
- 4.22 Mosaic MURA CA reconstructed slices of an 8 mm tumor from 12.5 % to 37.5 % depth, and each slice has a thickness of 1 mm : (a) reconstructed slice at 12.5 % depth of tumor using mask, (b) reconstructed slice at 12.5 % depth of tumor using antimask, (c) difference of (a) and (b), (d) reconstructed slice at 25 % depth of tumor using mask, (e) reconstructed slice at 25 % depth of tumor using antimask, (f) difference of (d) and (e) slices, (g) reconstructed slice at 37.5 % depth of tumor using mask, (h) reconstructed slice at 37.5 % depth of tumor using antimask, (i) difference of (g) and (h) slices. The TBR used is 10:1. 103
- 4.23 Mosaic MURA CA reconstructed slices of an 8 mm tumor from 50 % to 75 % depth, and each slice has a thickness of 1 mm : (a) reconstructed slice at 50 % depth of tumor using mask, (b) reconstructed slice at 50 % depth of tumor using antimask, (c)

| | | |
|------|--|-----|
| | difference of (a) and (b), (d) reconstructed slice at 62.5 % depth of tumor using mask, (e) reconstructed slice at 62.5 % depth of tumor using antimask, (f) difference of (d) and (e) slices, (g) reconstructed slice at 75 % depth of tumor using mask, (h) reconstructed slice at 75 % depth of tumor using antimask, (i) difference of (g) and (h) slices. The TBR used is 10:1. | 104 |
| 4.24 | Breast phantom reconstructed images using mosaic MURA mask/antimask with (a) 8 mm tumor, (b) 6 mm tumor, (c) 4 mm tumor and (d) 3 mm tumor. The TBR used is 10:1. | 105 |
| 4.25 | Breast phantom vertical profile through the center of tumor using mosaic MURA mask/antimask with a diameter of 8 mm (a) and 6 mm (b) | 106 |
| 4.26 | Breast phantom vertical profile through the center of tumor using mosaic MURA mask/antimask with a diameter of 4 mm (a) and 3 mm (b) | 107 |
| 4.27 | Breast phantom reconstructed images using mosaic MURA mask with (a) 8 mm tumor, (b) 6 mm tumor, (c) 4 mm tumor, and (d) 3 mm tumor diameter. The TBR used is 10:1 | 108 |
| 4.28 | Breast phantom vertical profile through the center of tumor using mosaic MURA mask with diameter of 8 mm (a), and 6 mm (b) | 109 |
| 4.29 | Breast phantom vertical profile through the center of tumor using mosaic MURA mask with a diameter of 4 mm (a) and 3 mm (b) | 110 |
| 4.30 | Mosaic MURA mask/antimask CA reconstructed slices of an 8 mm tumor from 12.5 % to 37.5 % depth, and each slice has a thickness of 1 mm : (a) reconstructed slice at 12.5 % depth of tumor using mask, (b) reconstructed slice at 12.5 % depth of tumor using antimask, (c) difference of (a) and (b), (d) reconstructed slice at 25 % depth of tumor using mask, (e) reconstructed slice at 25 % depth of tumor using antimask, (f) difference of (d) and (e) slices, (g) reconstructed slice at 37.5 % depth of tumor using mask, (h) reconstructed slice at 37.5 % depth of tumor using antimask, (i) difference of (g) and (h) slices. The TBR used is 5:1. | 111 |
| 4.31 | Breast phantom reconstructed images using mosaic MURA mask/antimask with (a) 8 mm tumor, (b) 6 mm tumor, (c) 4 mm tumor, and (d) 3 mm tumor diameter. The TBR used is 5:1 | 112 |
| 4.32 | Breast phantom vertical profile through the center of tumor using mosaic MURA mask/antimask with a diameter of 8 mm (a) and 6 mm (b). TBR 5:1 | 113 |

| | | |
|------|---|-----|
| 4.33 | Breast phantom vertical profile through the center of tumor using mosaic MURA mask/antimask with a diameter of 4 mm (a) and 3 mm (b). TBR 5:1 | 114 |
| 4.34 | Comparison of PSNR of MURA mask/antimask, mosaic MURA mask, and mosaic MURA mask/antimask for lesions of 8 mm, 6 mm, 4 mm, and 3 mm. TBR is 10:1. | 116 |
| 4.35 | Comparison of CBR of MURA mask/antimask, mosaic MURA mask, and mosaic MURA mask/antimask for lesions of 8 mm, 6 mm, 4 mm, and 3 mm. TBR is 10:1. | 116 |
| 4.36 | Comparison of MSE of MURA mask/antimask, mosaic MURA mask, and mosaic MURA mask/antimask for lesions of 8 mm, 6 mm, 4 mm, and 3 mm. TBR is 10:1. | 117 |
| 4.37 | Error bars of CBR and PSNR for mosaic MURA mask/antimask with TBR 10:1 | 118 |

LIST OF ABBREVIATIONS

| | |
|---------------------|---|
| μCi | Micro Curie |
| 2D | Two-dimensional |
| 3D | Three-dimensional |
| CA | Coded Aperture |
| CAI | Coded Aperture Imaging |
| CAIS | Coded Aperture Imaging System |
| CBR | Contrast-to-background Ratio |
| CNR | Contrast-to-Noise Ratio |
| cpm/ μCi | Counts per Minutes per μCi |
| CZT | Cadmium Zinc Telluride |
| FCFV | Fully Coded Field of View |
| FOV | Field of View |
| FWHM | Full Width at Half Maximum |
| GATE | Geant4 Application for Tomographic Emission |
| IAEA | International Atomic Energy Agency |
| keV | Kilo Electron Volt |
| LEGP | Low-Energy General-Purpose |
| LEHR | Low-Energy High-Resolution |
| LEHS | Low-Energy High-Sensitivity |
| LEUHR | Low-Energy Ultra-High-Resolution |
| LSF | Line Spread Function |
| MBq | Mega Becquerel |
| mCi | Milli Curie |
| MCNP5 | Monte Carlo N-Particle code version 5 |

| | |
|--------|---|
| MHC | Multihole Collimator |
| MIBI | Sestamibi |
| MLEM | Maximum Likelihood Expectation Maximization |
| MRI | Magnetic Resonance Imaging |
| MSE | Mean Square Error |
| MURA | Modified Uniformly Redundant Array |
| NaI | Sodium Iodide |
| NEMA | National Electrical Manufacturers Association |
| NFC | Near-field correction |
| NMSE | Normalized Mean Squared Error |
| OS-EM | Ordered Subsets Expectation-Maximization |
| PDF | Probability Density Function |
| PET | Positron Emission Tomography |
| PMT | Photomultiplier Tubes |
| PSF | Point Spread Function |
| PSNR | Peak Signal-to-Noise Ratio |
| PTRAC | Particle Track Output Card |
| RMSE | Root Mean Square Error |
| ROI | Region of Interest |
| SD | Standard Deviation |
| SNR | Signal-to-Noise Ratio |
| SPECT | Single Photon Emission Computed Tomography |
| TBR | Tumor-to-Background Ratio |
| Tc-99m | Technetium-99m |

CHAPTER 1

INTRODUCTION

1.1 Background

The first chapter is divided into six sections. The first section of this chapter focuses on the basics of breast cancer, detection and recognition, and imaging techniques that may help with a diagnosis. The second part provides a high-level overview of SPECT imaging, while the third explains the problem statement. The next three sections discuss the study goals and objectives, the scope and limitations, and the thesis contribution.

1.1.1 Breast Cancer

Cancer is a disease that starts with abnormal localized cell development and can infiltrate or spread to other areas of the body rapidly. There are several types of cancer that all start with the abnormal growth of cells that spread to adjacent regions of the body and/or spread to other organs beyond their normal limits. Worldwide, cancer cases are around 19.1 million (Sung et al., 2021), with the highest at 2.3 million cases of female breast cancer. The death recorded in 2020 worldwide due to cancer is 10.0 million, with 6.9% due to only breast cancer (Sung et al., 2021). Breast cancer is the most common type of cancer around the world. The other dominant types of cancers are colorectal, lung, liver, and stomach cancer. High-income countries have more than 90% comprehensive treatment availability for cancer patients, while low-income and developing countries have less than 15%, which causes an increase in the death rate (Miller et al., 2021; Siegel et al., 2020).

1.1.2 Detection and Recognition

The early detection of cancerous cells is vital for the successful treatment of the patient. Cancer is often diagnosed at a later stage when it has disrupted the functions of one or more critical organs and has spread throughout the body. Early detection methods are a hot area of current research. Detecting cancer cells in their earliest stages is the most crucial step in predicting the best prognosis. Several breast diagnostic techniques, including mammography, ultrasound, magnetic resonance imaging, single photon emission computed tomography, positron emission tomography, and biopsy, have been studied. However, these methods have substantial downsides, including being expensive, time-consuming, and unsuccessful for young women. It is crucial to create a method for early breast cancer diagnosis with high sensitivity and speed. In the United States and Europe, approximately one out of every eight women suffers from cancer at some point throughout their lives. In emerging nations, the overall frequency and death rate due to cancer has increased. However, breast cancer mortality has reduced in North America and the European Union (EU), owing mostly to early detection and effective systemic treatments. Although there is no obvious cause for breast cancer, some variables such as

smoking, obesity, lack of physical exercise, alcohol, infections, and molecular and genetic processes all raise the chance of the disease. Early identification techniques have been shown in clinical trials to increase survival rates by up to 5 years (L. Wang, 2017).

1.1.3 Breast Cancer Imaging Modalities

In order to collect and see the continuously expanding number of diverse medical structures with appropriate resolution and contrast, a constantly growing variety of image modalities with varied imaging capture parameters has been developed. In the last two decades, breast cancer detection and diagnosis have improved significantly. The two well-established modalities for breast cancer screening are mammography and ultrasound. The advancements in magnetic resonance imaging, nuclear medicine, and the hybrid of both modalities have also improved breast cancer characterization significantly. Each imaging modality has its own pros and cons. In Figure 1.1, the general breast imaging modalities are summarized (Bansal et al., 2013; Devi & Anandhamala, 2018; Glunde et al., 2009). The dotted box represents the current work carried out in this study.

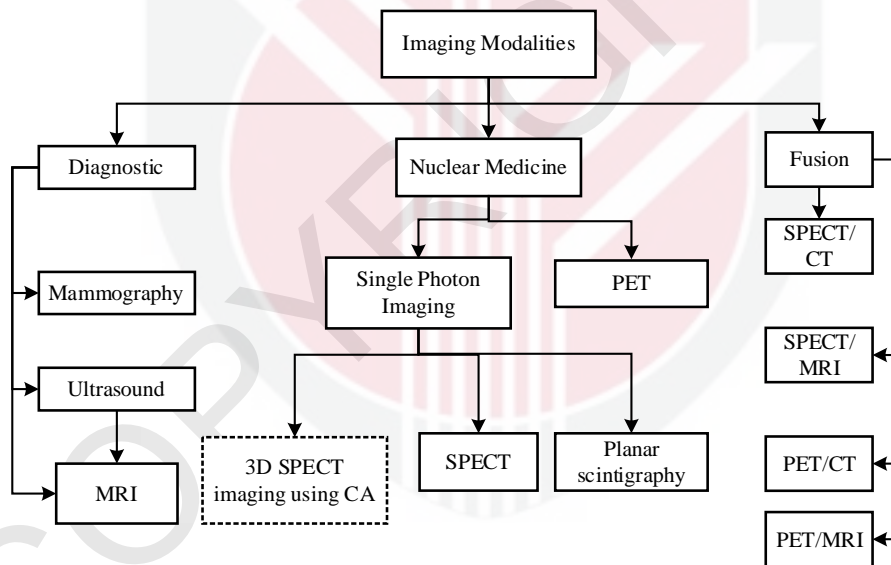


Figure 1.1: An overview of breast cancer imaging techniques

Mammography uses low-dose x-rays to examine the anatomical structures of the breast and detect any abnormalities. It has been excessively used and has been a gold standard for breast tumor imaging since 1960 (Devi & Anandhamala, 2018). However, factors such as breast density, age, infection stage, and family history can affect sensitivity and specificity (Shetty, 2010). As the breast density increases, it becomes more challenging to detect breast cancer using mammography. Mammography is not recommended for women under the age of 40 who have dense breasts or fibrocystic breasts. In

mammograms, dense breast tissue and cancer tumors have a similar appearance, making it difficult to discriminate between the two masses (Shareef et al., 2016).

Ultrasound is another important diagnostic imaging modality after mammography since it can further describe mammographically ambiguous masses. Ultrasound can diagnose high-risk patients and women with a dense pattern of breast parenchymal for whom mammography sensitivity is expected to be lower (Berg et al., 2008). With the advancement of the digital platform, this approach has seen a significant improvement in image resolution and detail. Ultrasound may be effective in distinguishing distinct tumors from benign nodularity in thick glandular breasts, especially in young patients. While a few relevant purposes include determining the difference between cystic and solid masses, as well as evaluating palpable lesions that are not evident on mammography (Kopans, 2004).

Magnetic resonance imaging is also used for breast cancer examination. It can detect the lesion which may be missed by mammography, but the chance of a false positive is there that can be minimized by using MRI with mammography (*Mammogram and Breast MRI: What's the Difference?*, n.d.). Many research topics have been investigated in order to choose individuals for biopsy while avoiding needless surgical operations. MRI and nuclear medicine imaging appear to be the most promising new breast imaging modalities (Saadatmand et al., 2019).

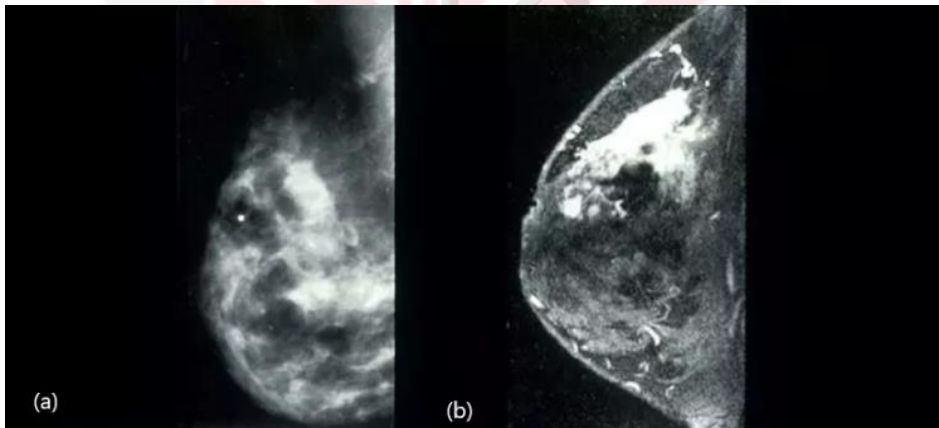


Figure 1.2: MRI has a high resolution, and it can be revealed by comparing (a) mammography screening with (b) MRI screening
(*Breast MRI Is Better than Mammography*, n.d.)

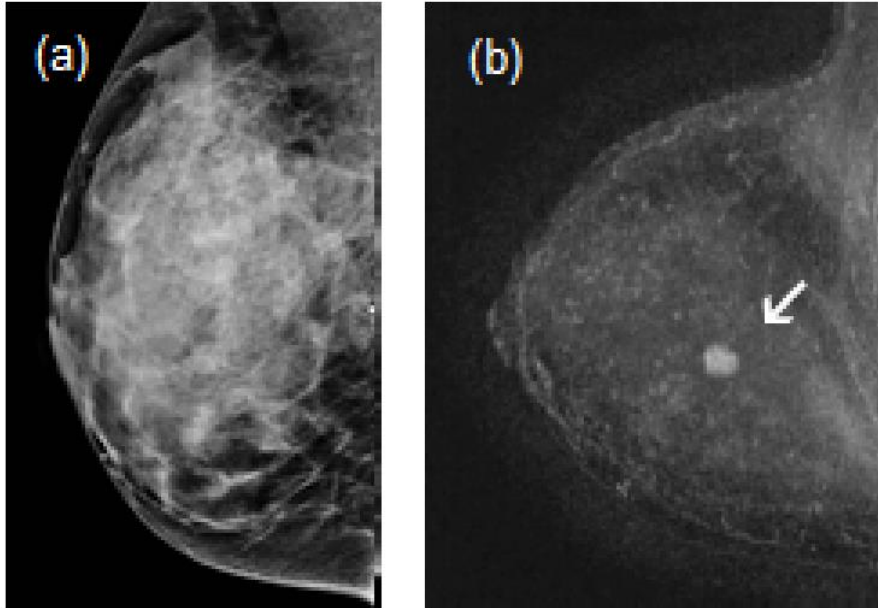


Figure 1.3: Mammography and MRI diagnosis, (a) mammography missed lesion, (b) while the lesion is clearly visible in MRI examination
(*Abbreviated Breast MRI Screening for Dense Breasts*, n.d.)

Nuclear medical imaging is a type of medical imaging that generates functional images of biological processes occurring at the cellular and subcellular levels. It works on the principle of a tracer. A pharmaceutical, which is a physiologically active ingredient, is chosen such that its spatial and temporal distribution throughout the body reflects a certain bodily function or metabolism. In the presence of a lesion, the medicine will be distributed unevenly throughout the body. The tracer is labeled with radionuclides that emit gamma rays or positrons in order to produce images of the radioactive tracer distribution. An external gamma camera sensitive to location can detect this radiation once the tracer has been administered to the patient, forming an image of the radionuclide distribution (Mózo, 2017).

Nuclear medicine, in comparison to previous imaging modalities, allows for highly sensitive measurements of a wide variety of biological processes. Single photon imaging (which includes SPECT and planar scintigraphy) and PET are the two most prevalent types of nuclear medicine imaging modalities.

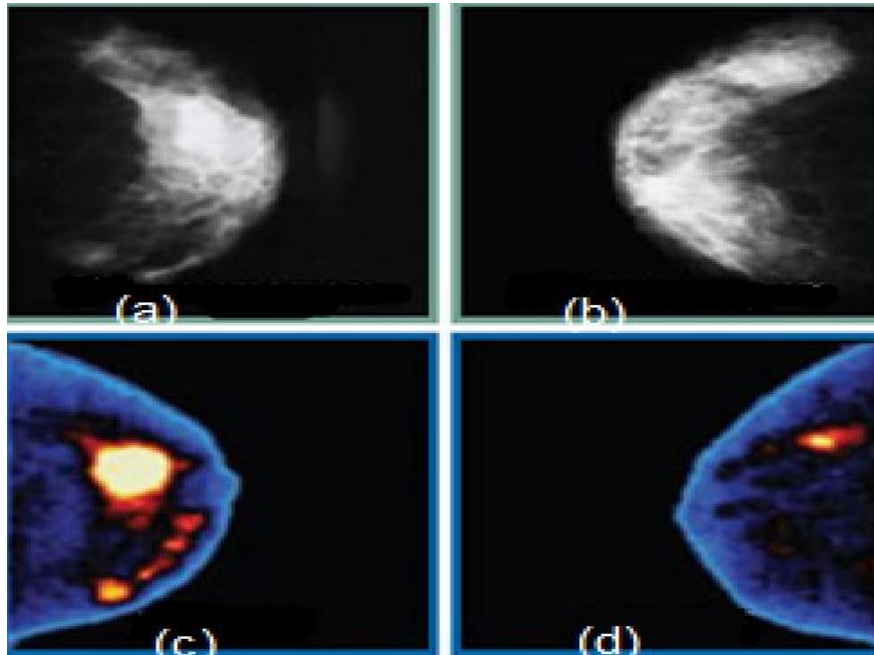


Figure 1.4: Gamma camera imaging vs. mammography, (a) left craniocaudal mammogram, (b) right craniocaudal mammogram, (c) left craniocaudal gamma imaging, and (d) right craniocaudal gamma imaging
(Breast Specific Gamma Imaging (BSGI), a New Imaging Modality, Proving Itself in Detecting Breast Cancer, n.d.)

From Figure 1.4, it can be seen that gamma imaging has a superior resolution for breast cancer detection than mammography. Mammography suffers from detection deficiency as the breast density increases, while gamma camera imaging can detect the breast lesion, thus proving superiority over mammography.

Breast scintigraphy, also known as scintimammography, is a nuclear medicine imaging method that employs radionuclides to examine malignant breast tumors. It involves the patient receiving a single-photon-emitting radiotracer and imaging using a gamma camera. The optimum scintimammography radiopharmaceuticals should have a high and selective tumor uptake with little action in the normal breast (Schillaci et al., 2008). Planar scintigraphy has been proven to be beneficial for evaluating patients with breast cancer, especially when mammography is inconclusive and in women with dense breasts (Schillaci & Buscombe, 2004). It has been used for over 40 years and is widely available in hospitals across the world. Planar scintigraphy, on the other hand, only has a high sensitivity for large tumors (Schillaci et al., 2007). Images of structures at one depth are generally covered by overlaid images of overlaying and underlying structures in the patient since it only offers a two-dimensional (2D) view of the patient from one specific perspective.

Unlike planar scintigraphy, breast SPECT imaging does not face overlapping structures in front or behind the imaging organ. Technetium-99m is a widely used diagnostic tool with highly accurate detection of cancerous cells.

1.2 SPECT Imaging Modality

The major categories of imaging modalities are structural or functional imaging based on the mechanism for providing physiological information about the organ being imaged as well as its own advantages and limitations. Among the functional modalities, SPECT and PET are state-of-the-art nuclear imaging modalities used for breast cancer diagnosis. However, SPECT, a non-invasive molecular imaging modality, is cheaper and widely used in modern hospitals. A lot of research has been done to advance the SPECT imaging system to reduce the mortality rate of breast cancer (Lakshmanan et al., 2016; Poma et al., 2019; Saad et al., 2011).

1.3 Problem Statement

SPECT imaging is undertaken using a parallel-hole collimator, but this technique suffers from clinical limitations as it has less reliability in detecting small lesions (less than one centimeter in diameter) due to trade-off between sensitivity and resolution. The collimation part of the SPECT camera for radioactive tracer distribution is the key part of the image formation that confines the particles into specific directions and stops the out-focused radiation depending upon the attenuation of the material within the energy window. The quality of the reconstructed images is severely affected by the design of the collimator as the hole, and septa size directly affects the sensitivity and resolution. Therefore, the collimator plays a vital role in the design of the SPECT gamma camera. Among the collimators, the multi-hole collimator is a commonly used collimator with thousands of holes to allow source particles to map unique points on the detector to form the image. However, MHC is so bulky and difficult to handle due to the high path length in the material and weight above 100 kg (Ogawa & Kato, 2002).

To address the weight of the collimator, two wire mesh collimator configurations were proposed as an alternative to the conventional multihole collimator (Saripan et al., 2007, 2009). The wire mesh collimators WMC1 and WMC2, made of wire grids, have reduced weights by 60.5% and 48.8% and have comparable performance to MHC.

The efficient alternative to the multihole collimator is a Coded Aperture (CA) for breast tumor investigation. The CA imaging technique was first introduced for high energy x- and gamma rays in far-field geometry in astronomy (Cannon & Fenimore, 1979; Fenimore & Cannon, 1978; Fenimore & Scientific, 1978; Gottesman & Fenimore, 1989). It was developed as a substitute for parallel hole collimators to improve spatial resolution and increase sensitivity while keeping the patient dose at a minimum. The CA mask is coupled with a standard clinical gamma camera in near-field imaging (M. A. Alnafea, 2021). The CA imaging technique used in nuclear medicine is due to its high sensitivity and signal-to-noise ratio (SNR) (Accorsi & Lanza, 2001; J. Wang & Zhao, 2021).

Moreover, its aim is to attain the high resolution of small pinholes while keeping the signal throughput high. The fundamental idea is to overcome photon scarcity by opening a large number of small pinholes rather than a single large one.

Varieties of coded mask designs, including binary fresnel zone plate, sinusoidal zone plate, L and X shaped array, non-redundant array, uniformly redundant array (URA), and modified uniformly redundant array (MURA) were investigated by Alnafea (M. A. Alnafea, 2018). It has been demonstrated that the FZP, non-redundant, X, and L-shaped have side lobes which cause image artifacts when used for reconstruction. Thus, these are not considered for clinical application as optimal design choices. However, the cyclic difference sets, such as URA's and MURA's, have been explored as the most promising patterns of coded aperture with high transmission characteristics (having 50% close/open area, i.e., the area transparent to gamma particles and opaque to gamma particles is same) and minimum side lobes. Moreover, the mosaic MURA, an anti-symmetric copy of the basic MURA patterns, exhibits better performance, especially when the object is a thick voxel source, and therefore, presents encouraging performance characteristics like resolution, contrast, and SNR as compared to MURA, and it also minimizes the background noise, the non-uniformity in the background.

Coded aperture-based SPECT imaging suffers from the noise that comes from various sources, including decoding algorithms, improper detector, and mask sampling, inappropriate shielding of detector and mask, background influence, and near-field artifacts (Accorsi & Lanza, 2001). For image reconstruction, different methods have been used, including convolution, correlation, and iterative reconstructions (Crockett & Fessler, 2021; Whiteley et al., 2021; Zeng, 2001; Zeniya et al., 2004). The image reconstruction using conventional correlation or convolution methods becomes noisy as the number of source points increases, while iterative reconstructions can still give a better-reconstructed image. The maximum likelihood expectation maximization (MLEM) iterative reconstruction is considered a better choice for coded aperture-based image reconstructions. However, 3D image reconstruction of the thick object is still challenging.

From the above discussion, the problem statement and research gap can be summarized below:

- The SPECT imaging is only carried out using a conventional multi-hole collimator. Although WMC1 and WMC2 were proposed, they offered reduced-weight collimator designs with comparable performance to that of the multi-hole collimator. The detection of a small lesion of less than 10 mm is still challenging using SPECT imaging camera commercially available.
- There has been no prior application of the mosaic MURA CA mask to 3D breast SPECT imaging. Mosaic MURA mask/antimask dual image reconstruction with maximum likelihood expectation maximization for 3D breast SPECT imaging was not achieved previously, let alone from only one projection.
- Reconstruction of 3D breast images from single projection is yet challenging. SPECT imaging with a multi-hole collimator uses a sinogram, a series of projections, to recreate a 3D image.

- The 3D breast imaging SPECT imaging systems using coded aperture technology are still under investigations.

1.4 Research Aims and Objectives

The primary objective of this research is to develop a 3D-coded aperture-based SPECT imaging system for early breast cancer detection. The system should be capable of reconstructing a 3D breast phantom with a minor lesion. GATE Monte Carlo software will be used to simulate the proposed SPECT imaging system. Moreover, maximum likelihood expectation maximization, an iterative algorithm, will be used for image reconstruction. The following goals have been established to achieve the aforementioned objective:

- To create and validate the simulated model of the SPECT SIEMENS Symbia T gamma camera using MCNP5 and GATE.
- To design a coded aperture mask and optimize an imaging system based on CA using a point source, a two-point source, and a planar source for performance improvement, including mask patterns, thickness, and magnification factor.
- To simulate and test a modified MLEM iterative reconstruction algorithm for reconstruction of real 3D breast phantom with tumors in various diameters and TBR system.

1.5 Scope and Limitation

This study demonstrates the viability of 3D SPECT image reconstruction employing coded aperture technology instead of parallel-hole collimator. Additionally, just one projection of the data taken from the patient's lateral position can be used for the 3D reconstruction of the breast phantom. Previously, coded aperture based imaging systems are mainly used for planar imaging and/or thin 3D imaging. Although the collimator-based SPECT scanners are available, they use sinograms by taking multiple projections from 360° angles around the patient and then can reconstruct a 3D image. The proposed SPECT camera using a coded aperture mask is a novel approach to the medical diagnosis of breast cancer patients. For the simulation of SPECT imaging camera, GATE Monte Carlo simulation software was used.

Significant effort was put into constructing a mosaic MURA mask used in the SPECT camera to simulate a female breast phantom. The mosaic MURA CA mask was designed using a basic 83 x 83 binary MURA and has dimensions of 16.6 x 16.6 x 0.15 cm³ with a fixed hole size of 1 mm² and is made of tungsten, which has almost 99.4% typical incident gamma attenuation at 140 keV energy. However, the scintillation detector was made of sodium iodide with thallium doping and had an area of 66.4 x 66.4 cm², and was filled with NaI material with a density of 3.67 g/cm³ and a thickness of 0.9525 cm. The backscattering compartment was made of Pyrex glass and had dimensions of 66.4 x 66.4 x 6.8 cm³.

For the aim of mimicking a clinical breast cancer examination, a half-ellipsoidal anthropomorphic breast phantom is used to approximate the realistic breast. In the center of the breast phantom is a lesion, and it is constructed by ductal networks, adipose tissues, glandular tissues, and skin. The objectives and limitations of this study are briefly discussed below.

The anthropomorphic breast phantom was simulated using a simulation setup with a mosaic MURA CA mask for 20 mCi activity. The mosaic MURA mask/antimask combined with MLEM iterative reconstruction generates a promising 3D breast image. The tumor size varied from 8 mm, 6 mm, 4 mm, and 3 mm, but activity, tumor depth, and TBR remained unchanged. Then, the experiments are repeated with TBR 5:1, and the reconstructed images are analyzed. The standard deviation of the 3D breast images was computed to assess and illustrate the error bars of the simulated tumor sizes. The statistical uncertainty reduces as the number of photon histories grows.

This investigation does not take into account the effect of background radiation. It is believed that the patient will be positioned in a lateral posture inside a breast housing chamber made of lead or tungsten. In this chamber, the patient's entire body, with the exception of the breast, will be shielded to prevent any background count contribution to the reconstruction of the image. The chest, heart, and lung radiation contribution is a subject of further work, which needs a bigger phantom and extensive computing resources.

The softwares used in this study are GATE, MCNP5, MATLAB, and Python. GATE and MCNP5 are used for simulating the SPECT camera, while MATLAB is used for the post-processing of the projection image to reconstruct the source object. Python is used to create variable parameter scripts that will be used to repeat the experiments.

1.6 Thesis Contribution

The most important contribution made by this study is the development of the SPECT imaging camera based on a coded aperture mask for 3D breast cancer detection. This SPECT imaging camera can reconstruct the 3D breast image from just a single angle of patient scanning data. No study deals with the SPECT imaging cameras based on coded aperture for the 3D breast phantom reconstruction. We developed a mosaic MURA CA mask and an anthropomorphic breast phantom to simulate the natural female breast. The details of research contributions are as follows:

- The development of the SIEMENS SPECT camera model in GATE and MCNP5 to validate the camera performance by comparing simulation results with the manufacturer's data.
- The MURA and mosaic MURA CA masks have been used within the breast phantom simulation. An extensive analysis was done using point sources, two-

point sources, and planar sources to optimize the performance of the CA imaging system.

- This study successfully developed a SPECT imaging system based on a coded aperture for 3D breast imaging and reconstructed the 3D image from a single projection instead of a sinogram. Moreover, the system “successfully detected lesion of 3 mm diameter”.
- A comparison among MURA mask/antimask, mosaic MURA mask, and mosaic MURA mask/antimask has been made by evaluating their performance from 3D breast phantom reconstructed images. The compressed anthropomorphic breast phantom is simulated with different lesion sizes and TBR for in-depth analysis. For image reconstruction MLEM iterative algorithm was used with mask/antimask.

REFERENCES

- Abbreviated Breast MRI Screening for Dense Breasts*. (n.d.). Retrieved August 8, 2022, from <https://radiologyregional.com/womens-diagnostic-and-breast-center/ab-mr-screening-for-dense-breasts/>
- Accorsi, R. (2001). *Design of a near-field coded aperture cameras for high-resolution medical and industrial gamma-ray imaging* (Doctoral dissertation, Massachusetts Institute of Technology).
- Accorsi, R., & Lanza, R. C. (2001). Near-field artifact reduction in planar coded aperture Imaging. *Applied Optics*, 40(26), 4697–4705. <https://doi.org/10.1364/ao.40.004697>
- Agostinelli, S., Allison, J., Amako, K. al, Apostolakis, J., Araujo, H., Arce, P., Asai, M., Axen, D., Banerjee, S., Barrand, G., others, Behner, F., Bellagamba, L., Boudreau, J., Broglia, L., Brunengo, A., Burkhardt, H., Chauvie, S., Chuma, J., ... Zschesche, D. (2003). GEANT4 - A simulation toolkit. *Nuclear Instruments and Methods in Physics Research, Section A: Accelerators, Spectrometers, Detectors and Associated Equipment*, 506(3), 250–303. [https://doi.org/10.1016/S0168-9002\(03\)01368-8](https://doi.org/10.1016/S0168-9002(03)01368-8)
- Alnafea, M. (2007). Coded aperture breast tumour imaging using a full-size clinical gamma camera. *PhD Thesis, University of Surrey, UK*. http://search.proquest.com.ezp.lib.unimelb.edu.au/docview/301672109?accountid=12372%0Ahttps://unimelb.hosted.exlibrisgroup.com/sfxlcl41/?url_ver=Z39.88-2004&rft_val_fmt=info:ofi/fmt:kev:mtx:dissertation&genre=dissertations+%26+theses&sid=ProQ:ProQuest+Dis
- Alnafea, M. A. (2017). An Innovative Concept of 3D X-Ray Imaging Systems for Painless Breast Cancer Detection. *New Perspectives in Breast Imaging*.
- Alnafea, M. A. (2021). *Non Monte Carlo Method for Intrinsic Investigation of the Potential Use of Modified Uniformly Redundant Arrays (Muras) Coded Apertures for Early Breast Tumor Imaging*. <https://doi.org/10.24966/NMRR-7419/100029>
- Alnafea, M. A., & Wells, K. (2018). Monte Carlo Simulation of Infinia Gamma Camera : A Verification and Validation Process. *Journal of Cancer Science and Therapy Volume 1/ Issue 10, 1(10)*, 1–14.
- Alnafea, M. A., Wells, K., Guy, M., & Spyrou, N. M. (2006). Near field corrections for coded aperture imaging in scintimammography. *IEEE Nuclear Science Symposium Conference Record*, 5, 2948–2953. <https://doi.org/10.1109/NSSMIC.2006.356494>
- Alnafea, M., Wells, K., Spyrou, N. M., & Guy, M. (2007). Preliminary Monte Carlo study of coded aperture imaging with a CZT gamma camera system for scintimammography. *Nuclear Instruments and Methods in Physics Research, Section A: Accelerators, Spectrometers, Detectors and Associated Equipment*, 573(1–2), 122–125. <https://doi.org/10.1016/j.nima.2006.11.007>

- Alnafea, M., Wells, K., Spyrou, N. M., Saripan, M. I., Guy, M., & Hinton, P. (2006). Preliminary results from a Monte Carlo study of breast tumour imaging with low-energy high-resolution collimator and a modified uniformly-redundant array-coded aperture. *Nuclear Instruments and Methods in Physics Research, Section A: Accelerators, Spectrometers, Detectors and Associated Equipment*, 563(1), 146–149. <https://doi.org/10.1016/j.nima.2006.01.124>
- Anger, H. O. (1952). Use of a Gamma-Ray Camera for in vivo Studies. *Nature Publishing Group*.
- Anger, H. O. (1958). Scintillation camera. *Review of Scientific Instruments*, 29(1), 27–33. <https://doi.org/10.1063/1.1715998>
- Arbab, A. S., Koizumi, K., Toyama, K., Arai, T., & Araki, T. (1998). Technetium-99m-tetrofosmin, Technetium-99m-MIBI and Thallium-201 uptake in rat myocardial cells. *Journal of Nuclear Medicine*, 39(2), 266–271.
- Assié, K., Breton, V., Buvat, I., Comtat, C., Jan, S., Krieguer, M., Lazaro, D., Morel, C., Rey, M., Santin, G., Simon, L., Staelens, S., Strul, D., Vieira, J. M., & Van De Walle, R. (2004). Monte Carlo simulation in PET and SPECT instrumentation using GATE. *Nuclear Instruments and Methods in Physics Research, Section A: Accelerators, Spectrometers, Detectors and Associated Equipment*, 527(1–2), 180–189. <https://doi.org/10.1016/j.nima.2004.03.117>
- Atomic, I., & Agency, E. (2004). IAEA Quality Control Atlas for Scintillation Camera Systems, 2003. *European Journal of Nuclear Medicine and Molecular Imaging*, 31(5), 760–760. <https://doi.org/10.1007/s00259-004-1461-9>
- Bahreyni Toossi, M. T., Islamian, J. P., Momennezhad, M., Ljungberg, M., & Naseri, S. H. (2010). SIMIND Monte Carlo simulation of a single photon emission CT. *Journal of Medical Physics*, 35(1), 42–47. <https://doi.org/10.4103/0971-6203.55967>
- Bakic, P. R., Pokrajac, D. D., De Caro, R., & Maidment, A. D. A. (2014). Realistic simulation of breast tissue microstructure in software anthropomorphic phantoms. *Lecture Notes in Computer Science (Including Subseries Lecture Notes in Artificial Intelligence and Lecture Notes in Bioinformatics)*, 8539 LNCS(3), 348–355. https://doi.org/10.1007/978-3-319-07887-8_49
- Bakic, P. R., Zhang, C., & Maidment, A. D. A. (2011). Development and characterization of an anthropomorphic breast software phantom based upon region-growing algorithm. *Medical Physics*, 38(6), 3165–3176. <https://doi.org/10.1118/1.3590357>
- Bansal, G. J., Thomas, K. G., & Lim, K. (2013). Imaging techniques in breast cancer. *Surgery (United Kingdom)*, 31(1), 15–21. <https://doi.org/10.1016/j.mpsur.2012.10.011>

- Baró, J., Sempau, J., Fernández-Varea, J. M., & Salvat, F. (1995). PENELOPE: An algorithm for Monte Carlo simulation of the penetration and energy loss of electrons and positrons in matter. *Nuclear Inst. and Methods in Physics Research, B*, 100(1), 31–46. [https://doi.org/10.1016/0168-583X\(95\)00349-5](https://doi.org/10.1016/0168-583X(95)00349-5)
- Barrett, H. H. (1972). Fresnel Zone Plate Imaging in Nuclear Medicine. *JOURNAL OF NUCLEAR MEDICINE*, 24(1), 2014–2015.
- Berg, W. A., Blume, J. D., Cormack, J. B., Mendelson, E. B., Lehrer, D., Böhm-Vélez, M., Pisano, E. D., Jong, R. A., Evans, W. P., Morton, M. J., Mahoney, M. C., Larsen, L. H., Barr, R. G., Farria, D. M., Marques, H. S., & Boparai, K. (2008). Combined screening with ultrasound and mammography vs mammography alone in women at elevated risk of breast cancer. *American Medical Association*, 299(18), 2151–2163. <https://doi.org/10.1001/jama.299.18.2151>
- Berrim, S., Lansiaart, A., & Moretti, J. L. (1996). Implementing of maximum likelihood in tomographical coded aperture. *IEEE International Conference on Image Processing*, 2, 745–748. <https://doi.org/10.1109/icip.1996.561004>
- Bhatti, S. N., & Sridhar-Keralapura, M. (2012). A novel breast software phantom for biomechanical modeling of elastography. *Medical Physics*, 39(4), 1748–1768. <https://doi.org/10.1118/1.3690467>
- Bhusal, N. (2019). Third Generation Gamma Camera SPECT System. *ArXiv*, August 2018.
- Bliznakova, K. (2018). Implementation of the module on anthropomorphic phantoms. *Anthropomorphic Phantoms in Image Quality and Patient Dose Optimization: A EUTEMPE Network Book*. <https://doi.org/10.1088/2053-2563/aae197ch1>
- Bliznakova, K., Bliznakov, Z., Bravou, V., Kolitsi, Z., & Pallikarakis, N. (2003). A three-dimensional breast software phantom for mammography simulation. *Physics in Medicine and Biology*, 48(22), 3699–3719.
- Bouhnik, J.-P., Garcia, T., Kudrolli, H., Levinson, C., Malmin, R., Miller, M., Motomura, N., Narayanan, M., Stearns, C., Vija, H., Wang, k. W., & Zeintl, I. J. (2018). NEMA Standards Publication NU 1-2018 Performance Measurements of Gamma Cameras. *Nema.Org*, 1–11.
- Breast Anatomy*. (n.d.). Retrieved August 23, 2022, from <https://www.mskcc.org/cancer-care/types/breast/anatomy-breast>
- Breast MRI is better than Mammography*. (n.d.). Retrieved August 8, 2022, from <https://healthmanagement.org/c/imaging/news/3-minute-breast-mri-better-than-mammography>
- Breast Specific Gamma Imaging (BSGI), a New Imaging Modality, Proving Itself in Detecting Breast Cancer*. (n.d.). Retrieved August 8, 2022, from https://www.medgadget.com/2009/02/new_imaging_modality_proving_itself_in_detecting_breast_cancer.html

- Busboom, A., Elders-Boll, H., Schotten, H. D., & A. BUSBOOM, H. ELDERS-BOLL, A. H. D. S. (1998). Uniformly redundant arrays. *Experimental Astronomy*, 8(2), 97–123. <https://doi.org/10.1023/A:1007966830741>
- Buvat, I., & Castiglioni, I. (2002). Monte Carlo simulations in SPET and PET. *Quarterly Journal of Nuclear Medicine*, 46(1), 48–61.
- Byard, K. (1993). Synthesis of binary arrays with perfect correlation properties - coded aperture imaging. *Nuclear Inst. and Methods in Physics Research, A*, 336(1–2), 262–268. [https://doi.org/10.1016/0168-9002\(93\)91107-X](https://doi.org/10.1016/0168-9002(93)91107-X)
- Caldwell, C. B., & Yaffe, M. J. (1990). Development of an anthropomorphic breast phantom. *Medical Physics*, 17(2), 273–280. <https://doi.org/10.1118/1.596506>
- Cannon, T. M., & Fenimore, E. E. (1979). Tomographical imaging using uniformly redundant arrays. *Applied Optics*, 18(7), 1052. <https://doi.org/10.1364/ao.18.001052>
- Carton, A.-K., Bakic, P., Ullberg, C., & Maidment, A. D. A. (2010). Development of a 3D high-resolution physical anthropomorphic breast phantom. *Medical Imaging 2010: Physics of Medical Imaging*, 7622, 762206. <https://doi.org/10.1117/12.845367>
- Carton, A. K., Bakic, P., Ullberg, C., Derand, H., & Maidment, A. D. A. (2011). Development of a physical 3D anthropomorphic breast phantom. *Medical Physics*, 38(2), 891–896. <https://doi.org/10.1118/1.3533896>
- Chen, B., Shorey, J., Saunders Jr, R. S., Richard, S., Thompson, J., Nolte, L. W., Samei, E., Saunders, R. S., Richard, S., Thompson, J., Nolte, L. W., Samei, E., Saunders Jr, R. S., Richard, S., Thompson, J., Nolte, L. W., Samei, E., Saunders, R. S., Richard, S., ... Samei, E. (2011). An Anthropomorphic Breast Model for Breast Imaging Simulation and Optimization. *Academic Radiology*, 18(5), 536–546. <https://doi.org/10.1016/j.acra.2010.11.009>
- Cherry, S. R., Sorenson, J. A., & Phelps, M. E. (2018). PHYSICS in NUCLEAR MEDICINE. In *Angewandte Chemie International Edition*, 6(11), 951–952. (Vol. 53, Issue 9). <https://doi.org/10.1017/CBO9781107415324.004>
- Cho, Z.-H. (1993). *Foundations of Medical Imaging*.
- Cieślak, M. J., Gamage, K. A. A., & Glover, R. (2016). Coded-aperture imaging systems: Past, present and future development – A review. *Radiation Measurements*, 92, 59–71. <https://doi.org/10.1016/j.radmeas.2016.08.002>
- Cole, E. B., Pisano, E. D., Kistner, E. O., Muller, K. E., Brown, M. E., Feig, S. A., Jong, R. A., Maidment, A. D. A., Staiger, M. J., Kuzmiak, C. M., Freimanis, R. I., Lesko, N., Rosen, E. L., Walsh, R., Williford, M., & Braeuning, M. P. (2003). Diagnostic accuracy of digital mammography in patients with dense breasts who underwent problem-solving mammography: Effects of image processing and lesion type. *Radiology*, 226(1), 153–160. <https://doi.org/10.1148/radiol.2261012024>

- Corporation, T. P. (1970). *Point Arrays Having Compact , Nonredundant Autocorrelations*. 61.
- Crockett, C., & Fessler, J. A. (2021). *Bilevel methods for image reconstruction*. <http://arxiv.org/abs/2109.09610>
- Cwikla, J. B., Buscombe, J. R., Kolasinska, A. D., Parbhoo, S. P., Thakrar, D. S., & Hilson, A. J. W. (1999). Correlation between uptake of Tc-99m SestaMIBI and prognostic factors of breast cancer. *Anticancer Research*, 19(3 B), 2299–2304.
- Darkhor, P., & Islamian, J. P. (2020). Review on recent developments in collimators of single photon emission computed tomography imaging. *Frontiers in Biomedical Technologies*, 7(2), 125–133. <https://doi.org/10.18502/fbt.v7i2.3859>
- de Vries, D. J., Moore, S. C., Zimmerman, R. E., Friedland, B., Mueller, S. P., & Lanza, R. C. (1990). Development and Validation of a Monte Carlo Simulation of Photon Transport in an Anger Camera. *IEEE Transactions on Medical Imaging*, 9(4), 430–438. <https://doi.org/10.1109/42.61758>
- Devi, R. R., & Anandhamala, G. S. (2018). Recent trends in medical imaging modalities and challenges for diagnosing breast cancer. *Biomedical and Pharmacology Journal*, 11(3), 1649–1658. <https://doi.org/10.13005/bpj/1533>
- Dicke, R. H. (1968). SCATTER-HOLE CAMERAS FOR X-RAYS AND GAMMA RAYS. *The Astrophysical Journal*, 153(2), 78–86.
- Digitizer and readout parameters*. (n.d.). Retrieved July 20, 2022, from https://opengate.readthedocs.io/en/latest/digitizer_and_detector_modeling.html
- Dondi, M., Palm, S., Busemann Sokole, E., Stodilka, R. Z., Wegst, a. V., & Zimmerman, R. E. (2009). Quality Assurance for SPECT Systems. *IAEA Human Health Series*. No. 6, 1–263. http://www-pub.iaea.org/MTCD/publications/PDF/Pub1394_web.pdf
- Dong, X., Saad, W. H. M., Adnan, W. A. W., Hashim, S., Hassan, N. P. za M., Nordin, A. J., & Saripan, M. I. (2013). Simulation of intrinsic resolution of scintillation camera in Monte Carlo environment. *IEEE ICSIPA 2013 - IEEE International Conference on Signal and Image Processing Applications*, 11–14. <https://doi.org/10.1109/ICSIPA.2013.6707969>
- Dong, X., Saripan, M., Mahmud, R., Mashohor, S., & Wang, A. (2018). Characterization of SIEMENS Symbia T SPECT camera in Monte Carlo simulation environment. *Pakistan Journal of Nuclear Medicine*, 8(1), 18–26. <https://doi.org/10.24911/pjnmed.175-1540569779>
- Du, Y., Frey, E. C., Wang, W. T., Tocharoenchai, C., Baird, W. H., & Tsui, B. M. W. (2002). Combination of MCNP and SimSET for Monte Carlo simulation of SPECT with medium- and high-energy photons. *IEEE Transactions on Nuclear Science*, 49 I(3), 668–674. <https://doi.org/10.1109/TNS.2002.1039547>

- ENERGY RESOLUTION*. (n.d.). Retrieved July 30, 2022, from <http://www.medimaging.gr/cd/pages/par3.htm>
- Erdi, Y. E. (2012). Limits of Tumor Detectability in Nuclear Medicine and PET. *Molecular Imaging and Radionuclide Therapy*, 21(2), 23–28. <https://doi.org/10.4274/mirt.138>
- Fenimore, E. E., & Cannon, T. M. (1978). Coded aperture imaging with uniformly redundant arrays. *Applied Optics*, 17(3), 337–347.
- Fenimore, E. E., & Cannon, T. M. (1981). Uniformly redundant arrays: digital reconstruction methods. *Applied Optics*, 20(10), 1858. <https://doi.org/10.1364/ao.20.001858>
- Fenimore, E. E., & Scientific, L. A. (1978). Coded aperture imaging: predicted performance of uniformly redundant arrays. *Applied Optics*, 17(22), 3562. <https://doi.org/10.1364/ao.17.003562>
- Filter Back Projection*. (n.d.). Retrieved August 14, 2022, from <https://radiopaedia.org/articles/filtered-back-projection-1>
- Flower, M. A. (2016). Webb's Physics of Medical Imaging, Second Edition. In *Webb's Physics of Medical Imaging, Second Edition*. <https://doi.org/10.1201/b12218>
- Fornalski, K. W. (2018). Simple empirical correction functions to cross sections of the photoelectric effect, Compton scattering, pair and triplet production for carbon radiation shields for intermediate and high photon energies. *Journal of Physics Communications*, 2(3). <https://doi.org/10.1088/2399-6528/aab408>
- Franco Cavalli, Stan B. Kaye, Heine H Hansen, James O Armitage, M. P.-G. (2013). *Textbook of Medical Oncology*.
- Frank Verhaegen, & Seco, J. (2022). Monte Carlo Techniques in Radiation Therapy. In *Taylor & Francis Group* (Issue 2nd).
- Gallicchio, L., Devasia, T. P., Tonorezos, E., Mollica, M. A., & Mariotto, A. (2022). Estimation of the number of Individuals living with metastatic cancer in the United States. *JNCI: Journal of the National Cancer Institute, Dja158*. <https://doi.org/10.1158/1055-9965.EPI-16-0889>
- Gao, S., Jia, B., Feng, G., Dong, C., Du, H., Bai, L., Zhong, Q., Ma, Q., Zeng, M., & Wang, F. (2020). First-in-human pilot study of an integrin $\alpha 6$ -targeted radiotracer for SPECT imaging of breast cancer. *Signal Transduction and Targeted Therapy*, 5(1), 2–4. <https://doi.org/10.1038/s41392-020-00266-9>
- General, M. A., Carlo, M., & Team, X.-M. C. (2003a). *LA-CP-03-0245*.
- General, M. A., Carlo, M., & Team, X.-M. C. (2003b). *LA-CP-03-0284*.

- Giaquinto, A. N., Miller, K. D., Tossas, K. Y., Winn, R. A., Jemal, A., & Siegel, R. L. (2022). Cancer statistics for African American/Black People 2022. *CA: A Cancer Journal for Clinicians*, 72(3), 202–229. <https://doi.org/10.3322/caac.21718>
- Giaquinto, A. N., Sung, H., Miller, K. D., Kramer, J. L., Newman, L. A., Minihan, A., Jemal, A., & Siegel, R. L. (2022). Breast cancer statistics, 2022. *A Cancer Journal for Clinicians*. <https://doi.org/10.3322/caac.21754>
- Glunde, K., Jacobs, M. A., Pathak, A. P., Artemov, D., & Bhujwala, Z. M. (2009). Molecular and functional imaging of breast cancer. *NMR in Biomedicine*, 22(1), 92–103. <https://doi.org/10.1002/nbm.1269>
- Goldstone, K. (1989). *Tissue Substitutes in Radiation Dosimetry and Measurement*, in: *ICRU Report 44, International Commission on Radiation Units and Measurements*. WB Saunders.
- Gopal B. Saha. (2006). Physics and Radiobiology of Nuclear Medicine. In *Springer Science+Business Media (Third)*. Springer.
- Gopal B. Saha, P. D., & Physics. (n.d.). *Physics and Radiobiology of Nuclear Medicine* (Issue Fourth Edition).
- Gottesman, S. R., & Fenimore, E. E. (1989). New family of binary arrays for coded aperture imaging. *Applied Optics*, 28(20), 4344. <https://doi.org/10.1364/ao.28.004344>
- GOURLAY, A. R., STEPHEN, J. B., & N.G.S.YOUNG. (1984). Geometrically designed coded aperture mask arrays. *Nuclear Instruments and Methods in Physics Research*, 13(3), 576.
- Gourlay, A. R., & Young, N. G. (1984). Coded aperture imaging: a class of flexible mask designs. *Applied Optics*, 23(22), 4111. <https://doi.org/10.1364/ao.23.004111>
- Hahn, L. J., & Kloiber, R. (1994). Three-Dimensional Restoration of Single Photon Emission Computed Tomography Images. *IEEE Transactions on Nuclear Science*, 41(5), 1746–1754. <https://doi.org/10.1109/23.317385>
- Hellfeld, D., Barton, P., Gunter, D., Haefner, A., Mihailescu, L., & Vetter, K. (2019). Real-Time Free-Moving Active Coded Mask 3D Gamma-Ray Imaging. *IEEE Transactions on Nuclear Science*, 66(10), 2252–2260. <https://doi.org/10.1109/TNS.2019.2939948>
- HINE, G. J. (1967). *INSTRUMENTATION IN NUCLEAR MEDICINE*. 1(8), 43–56.
- Hong, B., Mu, Z., & Liu, Y.-H. (2006). A new approach of 3D SPECT reconstruction for near-field coded aperture imaging. *Medical Imaging 2006: Physics of Medical Imaging*, 6142, 61424D. <https://doi.org/10.1117/12.653300>
- Hruska, C. B., & O'Connor, M. K. (2013). Nuclear imaging of the breast: Translating achievements in instrumentation into clinical use. *Medical Physics*, 40(5), 1–23.

- Hu, X., Nonomura, Y., & Kohno, M. (2011). Monte Carlo Simulation. *Journal of Biomedical Optics*, 16(12), 1057–1096. <https://www.ncbi.nlm.nih.gov/pubmed/22206261>
- Hubbell, J. H. (1999). Review of photon interaction cross section data in the medical and biological context. *Physics in Medicine and Biology*, 44(1). <https://doi.org/10.1088/0031-9155/44/1/001>
- Hubbell, J. H. (2006). Review and history of photon cross section calculations. *Physics in Medicine and Biology*, 51(13). <https://doi.org/10.1088/0031-9155/51/13/R15>
- Hubbell, J. H., Gimm, H. A., & O'Verbo, I. (1980). Pair, Triplet, and Total Atomic Cross Sections (and Mass Attenuation Coefficients) for 1 MeV to 100 GeV Photons in Elements Z=1 to 100. *Journal of Physical and Chemical Reference Data*, 9(4), 1023–1148. <https://doi.org/10.1063/1.555629>
- Iaea. (2006). Nuclear Medicine Resources Manual. *October*, 188–200.
- ICRP, A. (2009). ICRP Publication 110: adult reference computational phantoms. In *Ann. ICRP* (Vol. 39, Issue 2).
- International Atomic Energy Agency. (1984). *Quality Control of Nuclear Medicine Instruments*.
- Islami, F., Goding Sauer, A., Miller, K. D., Siegel, R. L., Fedewa, S. A., Jacobs, E. J., McCullough, M. L., Patel, A. V., Ma, J., Soerjomataram, I., Flanders, W. D., Brawley, O. W., Gapstur, S. M., & Jemal, A. (2018). Proportion and number of cancer cases and deaths attributable to potentially modifiable risk factors in the United States. *CA: A Cancer Journal for Clinicians*, 68(1), 31–54. <https://doi.org/10.3322/caac.21440>
- Jan, S. bastien, Santin, G., Strul, D., Staelens, S., Assie, K and Autret, D and Avner, S and Barbier, R and Bardies, M and Bloomfield, P. and others, Jan, S. bastien, Benoit, D., Becheva, E., Lin, H., Chuang, K., Lin, Y., Pet, C., España, S., Herraiz, J. L., Vicente, E., Lazaro, D., Buvat, I., Loudos, G., Santin, G., ... Morel, C. (2004). GATE : a simulation toolkit for PET and SPECT. *Physics in Medicine and Biology*, 49(19), 4543. <https://doi.org/10.1088/0031-9155/49/19/007>
- Jeong, M., & Hammig, M. D. (2020). Comparison of gamma ray localization using system matrixes obtained by either MCNP simulations or ray-driven calculations for a coded-aperture imaging system. *Nuclear Instruments and Methods in Physics Research, Section A: Accelerators, Spectrometers, Detectors and Associated Equipment*, 954(October 2018), 161353. <https://doi.org/10.1016/j.nima.2018.10.031>
- Jeong, M., & Kim, G. (2021). MCNP-polimi simulation for the compressed-sensing based reconstruction in a coded-aperture imaging CAI extended to partially-coded field-of-view. *Nuclear Engineering and Technology*, 53(1), 199–207. <https://doi.org/10.1016/j.net.2020.02.011>

- Jeong, M., Van, B., Wells, B. T., D'Aries, L. J., & Hammig, M. D. (2018). Scalable gamma-ray camera for wide-area search based on silicon photomultipliers array. *Review of Scientific Instruments*, 89(3). <https://doi.org/10.1063/1.5016563>
- Jiang, S., Member, S., Wu, Z., Ma, T., & Jin, Y. (2004). *Design of Coded Aperture Collimator for High- resolution & High-sensitivity MicroSPECT*. 00(1), 2980–2984.
- Jonasson, T. (2003). Revival of a Gamma Camera. *Nuclear Physics*.
- Joshi, S. (2014). *Coded Aperture Imaging Applied to Pixelated CdZnTe detectors*. 9. <https://cztlab.engin.umich.edu/wp-content/uploads/sites/187/2015/03/Sonal.pdf>
- Kadri, O., & Alfuraih, A. (2019). Monte Carlo assessment of coded aperture tool for breast imaging: a Mura-mask case study. *Nuclear Science and Techniques*, 30(11). <https://doi.org/10.1007/s41365-019-0682-3>
- Kijewski, M. F. (2016). Positron Emission Tomography (PET) and Single-Photon Emission Computed Tomography (SPECT) Physics. In *Handbook of Neuro-Oncology Neuroimaging: Second Edition* (Second Edi). Elsevier. <https://doi.org/10.1016/B978-0-12-800945-1.00032-X>
- Knottenbelt, D. C., Bvm, O. B. E., Dvm, S., & Mrcvs, S. D. E. (2015). *Gamma Scintigraphy Nuclear medicine and radiopharmaceuticals for molecular diagnosis*.
- Kopans, D. B. (2004). Sonography Should Not Be Used for Breast Cancer Screening until Its Efficacy Has Been Proven Scientifically. *American Journal of Roentgenology*, 182(2), 489–491. <https://doi.org/10.2214/ajr.182.2.1820489>
- Lakshmanan, M. N., Morris, R. E., Greenberg, J. A., Samei, E., & Kapadia, A. J. (2016). Coded aperture coherent scatter imaging for breast cancer detection: a Monte Carlo evaluation. *Medical Imaging 2016: Physics of Medical Imaging*, 9783, 978321. <https://doi.org/10.1117/12.2216482>
- Laptev, A., & Perry, R. (2017). Simplification of an MCNP model designed for dose rate estimation. *EPJ Web of Conferences*, 153, 1–8. <https://doi.org/10.1051/epjconf/201715306018>
- Lazaro, D., El Bitar, Z., Breton, V., Hill, D., & Buvat, I. (2005). Fully 3D Monte Carlo reconstruction in SPECT: A feasibility study. *Physics in Medicine and Biology*, 50(16), 3739–3754. <https://doi.org/10.1088/0031-9155/50/16/006>
- Lee, T., Lee, H., & Lee, W. (2020). Coded aperture imager with depth of interaction scintillators. *Nuclear Instruments and Methods in Physics Research, Section A: Accelerators, Spectrometers, Detectors and Associated Equipment*, 954(December 2018). <https://doi.org/10.1016/j.nima.2019.01.010>

- Lee, Y. J., Ryu, H. J., Cho, H. M., Lee, S. W., Choi, Y. N., & Kim, H. J. (2013). Simulation studies of a high resolution SPECT system for a photon counting semiconductor detector. *IFMBE Proceedings*, 39 *IFMBE*, 1068–1071. https://doi.org/10.1007/978-3-642-29305-4_280
- Levin, A., Fergus, R., Durand, F., & Freeman, W. T. (2007). Image and depth from a conventional camera with a coded aperture. *ACM Transactions on Graphics*, 26(99), 70. <https://doi.org/10.1145/1239451.1239521>
- Liu, H., Zhan, H., Sun, D., & Zhang, Y. (2020). Comparison of BSGI, MRI, mammography, and ultrasound for the diagnosis of breast lesions and their correlations with specific molecular subtypes in Chinese women. *BMC Medical Imaging*, 20(1), 1–10. <https://doi.org/10.1186/s12880-020-00497-w>
- Liu, Q., Cheng, Y., Yang, Y., Peng, Y., Li, H., Xiong, Y., & Zhu, T. (2020). Image reconstruction using multi-energy system matrices with a scintillator-based gamma camera for nuclear security applications. *Applied Radiation and Isotopes*, 163(October 2019), 109217. <https://doi.org/10.1016/j.apradiso.2020.109217>
- M. A. Alnafea. (2018). A Review of Coded Aperture Families having Perfect Mathematical Imaging Properties used for Near Field Imaging Application. *Asian Journal of Medical and Health Research*, 3(07). www.ajmhr.com
- Mammogram and Breast MRI: What's the Difference?* (n.d.). Retrieved April 16, 2022, from <https://www.verywellhealth.com/difference-between-a-mammogram-and-a-breast-mri-430274>
- Martineau, A., Rocchisani, J. M., & Moretti, J. L. (2010). Coded aperture optimization using Monte Carlo simulations. *Nuclear Instruments and Methods in Physics Research, Section A: Accelerators, Spectrometers, Detectors and Associated Equipment*, 616(1), 75–80. <https://doi.org/10.1016/j.nima.2010.02.261>
- Meikle, S. R., Fulton, R. R., Eberl, S., Dahlbom, M., Wong, K. P., & Fulham, M. J. (2001). An investigation of coded aperture imaging for small animal SPECT. *IEEE Transactions on Nuclear Science*, 48(3), 816–821. <https://doi.org/10.1109/23.940169>
- Mertz, L., & Young, N. O. (1996). *Fresnel Transformations of Images*.
- MI, S. (2018). Optimizing Breast Cancer Images from Wire Mesh Collimator SPECT Camera Using Characterized Butterworth Filter. *International Journal of Nuclear Medicine & Radioactive Substances*, 1(1), 1–10.
- Michael, A. (2012). Monte Carlo Calculations in Nuclear Medicine. In *Monte Carlo Calculations in Nuclear Medicine*. <https://doi.org/10.1201/b13073>
- Miller, K. D., Ortiz, A. P., Pinheiro, P. S., Bandi, P., Minihan, A., Fuchs, H. E., Martinez Tyson, D., Tortolero-Luna, G., Fedewa, S. A., Jemal, A. M., & Siegel, R. L. (2021). Cancer statistics for the US Hispanic/Latino population, 2021. *CA: A Cancer Journal for Clinicians*, 71(6), 466–487.

- Mokri, S. S., Saripan, M. I., Abd Rahni, A. A., Nordin, A. J., Hashim, S., & Marhaban, M. H. (2016). PET Image Reconstruction Incorporating 3D Mean-Median Sinogram Filtering. *IEEE Transactions on Nuclear Science*, 63(1), 157–169. <https://doi.org/10.1109/TNS.2015.2513484>
- Mowlavi, A. A., Najafabadi, R. I., & Faygh, R. K. (2005). Calculation of Intrinsic Efficiency of NaI(Tl) Detector Using MCNP Code. *International Journal of Pure and Applied Physics*, 1(2), 129–136. <http://www.ripublication.com>
- Mózo, B. S. (2017). Acceleration of GATE Monte Carlo Simulations. In *Journal of Chemical Information and Modeling* (Vol. 53, Issue 9). <file:///C:/Users/User/Downloads/fvm939e.pdf>
- Mu, Z., Dobrucki, L. W., & Liu, Y. H. (2016). SPECT imaging of 2-D and 3-D distributed sources with near-field coded aperture collimation: Computer simulation and real data validation. *Journal of Medical and Biological Engineering*, 36(1), 32–43. <https://doi.org/10.1007/s40846-016-0111-6>
- Mu, Z., Dobrucki, W. L., Hu, X., & Liu, Y. H. (2010). Recent progress on SPECT imaging with near-field coded aperture collimation: A small animal study. *IEEE Nuclear Science Symposium Conference Record, October*, 3450–3453. <https://doi.org/10.1109/NSSMIC.2010.5874447>
- Mu, Z., Hong, B., Li, S., & Liu, Y. H. (2009). A novel three-dimensional image reconstruction method for near-field coded aperture single photon emission computerized tomography. *Medical Physics*, 36(5), 1533–1542. <https://doi.org/10.1118/1.3103490>
- Mu, Z., & Liu, Y.-H. H. (2006). Aperture collimation correction and maximum-likelihood image reconstruction for near-field coded aperture imaging of single photon emission computerized tomography. *IEEE Transactions on Medical Imaging*, 25(6), 701–711. <https://doi.org/10.1109/TMI.2006.873298>
- Murphy, W. A. (2002). Practical Breast Pathology. In *American Journal of Roentgenology* (Vol. 179, Issue 4). <https://doi.org/10.2214/ajr.179.4.1790900>
- Muzahir, S. (2020). Molecular Breast Cancer Imaging in the Era of Precision Medicine. *American Journal of Roentgenology*, 215(6), 1512–1519. <https://doi.org/10.2214/AJR.20.22883>
- Odinaka, I., O Sullivan, J. A., Politte, D. G., MacCabe, K. P., Kaganovsky, Y., Greenberg, J. A., Lakshmanan, M., Krishnamurthy, K., Kapadia, A. J., Carin, L., & Brady, D. J. (2017). Joint System and Algorithm Design for Computationally Efficient Fan Beam Coded Aperture X-Ray Coherent Scatter Imaging. *IEEE Transactions on Computational Imaging*, 3(4), 506–521. <https://doi.org/10.1109/tci.2017.2721742>
- Ogawa, K., & Kato, J. (2002). Collimator Design for Single Photon Emitter. *IEEE Nuclear Science Symposium and Medical Imaging Conference*, 2, 760–763. <https://doi.org/10.1109/nssmic.2002.1239434>

- Ogawa, K., & Kato, J. (2003). Wired Collimator for Single Photon Emitter. *IEEE Transactions on Nuclear Science*, 50(5 II), 1536–1540. <https://doi.org/10.1109/TNS.2003.817949>
- Park, S., Boo, J., Hammig, M., & Jeong, M. (2021). Impact of aperture-thickness on the real-time imaging characteristics of coded-aperture gamma cameras. *Nuclear Engineering and Technology*, 53(4), 1266–1276. <https://doi.org/10.1016/j.net.2020.09.012>
- Paul, E. S. (2019). *Analysis of Transform-Based Compression Techniques for MRI and CT Images*.
- Peter F. Sharp, H. G. G. and A. D. M. (2015). Practical nuclear medicine., In *Syria Studies* (Vol. 7, Issue 1). https://www.researchgate.net/publication/269107473_What_is_governance/link/548173090cf22525dcb61443/download%0Ahttp://www.econ.upf.edu/~reynal/Civil_wars_12December2010.pdf%0Ahttps://think-asia.org/handle/11540/8282%0Ahttps://www.jstor.org/stable/41857625
- Peterson, T. E., & Furenlid, L. R. (2011). SPECT detectors: The Anger Camera and beyond. *Physics in Medicine and Biology*, 56(17). <https://doi.org/10.1088/0031-9155/56/17/R01>
- Photoelectric Effect*. (n.d.). Retrieved August 13, 2022, from <https://www.nuclear-power.com/nuclear-power/reactor-physics/interaction-radiation-matter/interaction-gamma-radiation-matter/photoelectric-effect/>
- PinHole camera model*. (n.d.). Retrieved July 28, 2022, from https://en.wikipedia.org/wiki/Pinhole_camera_model
- Pokrajac, D. D., Maidment, A. D. A., & Bakic, P. R. (2012). Optimized generation of high resolution breast anthropomorphic software phantoms. *Medical Physics*, 39(4), 2290–2302. <https://doi.org/10.1118/1.3697523>
- Poma, G. E., Garibaldi, F., Giuliani, F., Insero, T., Lucentini, M., Marcucci, A., Musico, P., Petta, C., Santavenere, F., Sutura, C., & Cisbani, E. (2019). Monte Carlo simulations of an innovative molecular breast imaging system for the small breast cancer diagnosis using GATE. *Radiation Effects and Defects in Solids*, 174(11–12), 1008–1019. <https://doi.org/10.1080/10420150.2019.1683839>
- Prionas, N. D., Burkett, G. W., & McKenney, S. E. (2005). Development of a Patient-Specific Two-Compartment Anthropomorphic Breast Phantom. *Bone*, 23(1), 1–7. <https://doi.org/10.1088/0031-9155/57/13/4293.Development>
- Proctor, R. J., Skinner, G. K., & Willmore, A. P. (1979). *The design of optimum coded mask X-ray telescopes*.
- Rai, S., Ravi, M., K, V. S., & S, S. S. S. (2016). *GATE Simulation of Coded Mask Aperture for near field gamma ray imaging application*. 61, 1088–1089.

- Rodrigues, S., Tome, B., Abreu, M. C., Santos, N., Mendes, P. R., & Peralta, L. (2007). *Monte Carlo Simulation and Experimental Characterization of a Dual Head Gamma Camera*. 1–11. <http://arxiv.org/abs/0711.2577>
- Russo, P., Di Lillo, F., Corvino, V., Frallicciardi, P. M., Sarno, A., & Mettivier, G. (2020). CdTe compact gamma camera for coded aperture imaging in radioguided surgery. *Physica Medica*, 69(December 2019), 223–232. <https://doi.org/10.1016/j.ejmp.2019.12.024>
- Saad, W. H. M. M., Roslan, R. E., Mahdi, M. A., Choong, W.-S. S., Saion, E., & Saripan, M. I. (2011). Monte Carlo design of optimal wire mesh collimator for breast tumor imaging process. *Nuclear Instruments and Methods in Physics Research, Section A: Accelerators, Spectrometers, Detectors and Associated Equipment*, 648(1), 254–260. <https://doi.org/10.1016/j.nima.2011.05.064>
- Saadatmand, S., Geuzinge, H. A., Rutgers, E. J. T., Mann, R. M., de Roy van Zuidewijn, D. B. W., Zonderland, H. M., Tollenaar, R. A. E. M., Lobbes, M. B. I., Ausems, M. G. E. M., van 't Riet, M., Hooning, M. J., Mares-Engelberts, I., Luiten, E. J. T., Heijnsdijk, E. A. M., Verhoef, C., Karssemeijer, N., Oosterwijk, J. C., Obdeijn, I. M., de Koning, H. J., ... van Druten, E. (2019). MRI versus mammography for breast cancer screening in women with familial risk (FaMRIsc): a multicentre, randomised, controlled trial. *The Lancet Oncology*, 20(8), 1136–1147. [https://doi.org/10.1016/S1470-2045\(19\)30275-X](https://doi.org/10.1016/S1470-2045(19)30275-X)
- Saripan, M. I., Hashim, S., Mashohor, S., Adnan, W. A. W., & Marhaban, M. H. (2008). Characteristics of multihole collimator gamma camera simulation modeled using MCNP5. *AIP Conference Proceedings*, 1017, 205–209. <https://doi.org/10.1063/1.2940628>
- Saripan, M. I., Mohd Saad, W. H., Hashim, S., Mahmud, R., Nordin, A. J., & Mahdi, M. A. (2009). Monte carlo simulation on breast cancer detection using wire mesh collimator gamma camera. *IEEE Transactions on Nuclear Science*, 56(3), 1321–1324. <https://doi.org/10.1109/TNS.2008.2012058>
- Saripan, M. I., Petrou, M., & Wells, K. (2007). Design of a wire-mesh collimator for gamma cameras. *IEEE Transactions on Biomedical Engineering*, 54(9), 1598–1612. <https://doi.org/10.1109/TBME.2007.902584>
- Schellingerhout, D., Accorsi, R., Mahmood, U., Idoine, J., Lanza, R. C., & Weissleder, R. (2002). Coded aperture nuclear scintigraphy: A novel small animal imaging technique. *Molecular Imaging*, 1(4), 344–353. <https://doi.org/10.1162/153535002321093954>
- Schillaci, O., & Buscombe, J. R. (2004). Breast scintigraphy today: Indications and limitations. *European Journal of Nuclear Medicine and Molecular Imaging*, 31(SUPPL. 1). <https://doi.org/10.1007/s00259-004-1525-x>
- Schillaci, O., Danieli, R., Filippi, L., Romano, P., Cossu, E., Manni, C., & Simonetti, G. (2007). Scintimammography with a hybrid SPECT/CT imaging system. *Anticancer Research*, 27(1 B), 557–562.

- Schillaci, O., Spanu, A., & Madeddu, G. (2008). Breast scintigraphy. *Cancer Imaging*, 417–422. <https://doi.org/10.1016/B978-012374212-4.50046-8>
- Schwarz, A., Shemer, A., Danan, Y., Bar-Shalom, R., Avraham, H., Zlotnik, A., & Zalevsky, Z. (2020). Gamma radiation imaging system via variable and time-multiplexed pinhole arrays. *Sensors (Switzerland)*, 20(11), 1–14. <https://doi.org/10.3390/s20113013>
- Shareef, M., Ashraf, M. A., & Sarfraz, M. (2016). Natural cures for breast cancer treatment. *Saudi Pharmaceutical Journal*, 24(3), 233–240. <https://doi.org/10.1016/j.jsps.2016.04.018>
- Shetty, M. K. (2010). Screening for Breast Cancer with Mammography: Current Status and An Overview. *Indian Journal of Surgical Oncology*, 1(3), 218–223. <https://doi.org/10.1007/s13193-010-0014-x>
- Shorey, J. (2007). Stochastic simulations for the detection of objects in three dimensional volumes: Applications in medical imaging and ocean acoustics. *ProQuest Dissertations and Theses*, 257. https://ru.idm.oclc.org/login?url=http://search.proquest.com/docview/304868435?accountid=11795%5Cnhttp://ru.on.worldcat.org/atoztitles/link?sid=ProQ:&issn=&volume=&issue=&title=*Stochastic+simulations+for+the+detection+of+objects+in+three%0Adimensional+vo
- Shultis, J. K., & Faw, R. E. (2002). *FUNDAMENTALS OF NUCLEAR SCIENCE AND ENGINEERING*.
- Siegel, R. L., Miller, K. D., & Jemal, A. (2020). Cancer statistics, 2020. *CA: A Cancer Journal for Clinicians*, 70(1), 7–30. <https://doi.org/10.3322/caac.21590>
- Siemens. (2013). *Symbia T Series*. 20. https://static.healthcare.siemens.com/siemens_hwem-hwem_sxxa_websites-context-root/wcm/idc/groups/public/@us/@imaging/@molecular/documents/download/mda1/mdkw/~edisp/symbia-t-spec-sheet-2010-01977049.pdf
- Simpkin, D. J. (1999). The AAPM/RSNA physics tutorial for residents: Radiation interactions and internal dosimetry in nuclear medicine. *Radiographics*, 19(1), 155–167. <https://doi.org/10.1148/radiographics.19.1.g99ja18155>
- Simpson, R. G., & Barrett, H. H. (1980). Coded-Aperture Imaging. In *In: Nudelman, S., Patton, D.D. (eds) Nuclear Medicine, Ultrasonics, and Thermography*. Springer, Boston, MA. https://doi.org/https://doi.org/10.1007/978-1-4684-3671-6_8
- Skinner, G. K. (1984). Imaging with coded-aperture masks. *Nuclear Instruments and Methods In Physics Research*, 221(1), 33–40. [https://doi.org/10.1016/0167-5087\(84\)90174-1](https://doi.org/10.1016/0167-5087(84)90174-1)
- SPECT imaging applications to myocardial perfusion and brain imaging*. (n.d.). Retrieved August 8, 2022, from <https://openmedscience.com/spect-imaging/>

- Staelens, S., & Buvat, I. I. I. (2009). Monte Carlo Simulations in Nuclear Medicine Imaging. In *Advances in Biomedical Engineering*. Elsevier. <https://doi.org/10.1016/B978-0-444-53075-2.00005-8>
- Staelens, S., Strul, D., Santin, G., Vandenberghe, S., Koole, M., D'Asseler, Y., Lemahieu, I., & Van de Walle, R. (2003). Monte Carlo simulations of a scintillation camera using GATE: Validation and application modelling. *Physics in Medicine and Biology*, 48(18), 3021–3042. <https://doi.org/10.1088/0031-9155/48/18/305>
- Starfiel, D. M. (2009). Towards clinically useful coded apertures for planar nuclear medicine imaging. *Physics in Medicine and Biology*, 36(4), 125–133. <https://doi.org/10.1016/j.apradiso.2020.109217%0Ahttps://he-www.harvard.edu/HREXI/intro/1998..Exp..Astr..8..97..Busboom..URAs.pdf>
- Stute, S., Carlier, T., Cristina, K., Noblet, C., Martineau, A., Hutton, B., Barnden, L., & Buvat, I. (2011). Monte Carlo simulations of clinical PET and SPECT scans: Impact of the input data on the simulated images. *Physics in Medicine and Biology*, 56(19), 6441–6457. <https://doi.org/10.1088/0031-9155/56/19/017>
- Sung, H., Ferlay, J., Siegel, R. L., Laversanne, M., Soerjomataram, I., Jemal, A., & Bray, F. (2021). Global Cancer Statistics 2020: GLOBOCAN Estimates of Incidence and Mortality Worldwide for 36 Cancers in 185 Countries. *CA: A Cancer Journal for Clinicians*, 71(3), 209–249. <https://doi.org/10.3322/caac.21660>
- Team, X.-5 M. C. (2003). MCNP — A General Monte Carlo N-Particle Transport Code, Version 5, Volume I: Overview and Theory. *Los Alamos National Laboratory, Los Alamos, 1*.
- Vassilieva, O. I., & Chaney, R. C. (2002). Method for reducing background artifacts from images in single-photon emission computed tomography with a uniformly redundant array coded aperture. *Applied Optics*, 41(7), 1454. <https://doi.org/10.1364/ao.41.001454>
- Vieira, L., Vaz, T. F., Costa, D. C., & Almeida, P. (2014). Monte Carlo simulation of the basic features of the GE Millennium MG single photon emission computed tomography gamma camera. *Revista Espanola de Medicina Nuclear e Imagen Molecular*, 33(1), 6–13. <https://doi.org/10.1016/j.remnm.2013.03.009>
- Voxelized source and phantom*. (n.d.). Retrieved September 6, 2022, from https://opengate.readthedocs.io/en/latest/voxelized_source_and_phantom.html#voxelized-sources
- Vučina, J., Nikolić, N., & Petrović, D. (2009). Technetium-99m in production and use. *Nuclear Technology and Radiation Protection*, 24(1), 68–73. <https://doi.org/10.2298/NTRP0901068V>

- Wackers, F. J. T., Berman, D. S., Watson, D. D., Beller, G. A., Strauss, H. W., Boucher, C. A., Picard, M., Holman, B. L., Fridrich, R., Inglese, E., Delaloye, B., Bischof-delaloye, A., Camin, L., & Mckusick, K. (1989). Technetium-99m hexakis 2-methoxyisobutyl Isonitrile: Human Biodistribution, Dosimetry, Safety, and Preliminary Comparison to Thallium-201 for Myocardial Perfusion Imaging. *Journal of Nuclear Medicine: Official Publication, Society of Nuclear Medicine*, 30(3), 301–311.
- Wahl, C. G., Brown, S., Kaye, W., Moran, K., Zhang, F., Sowers, J., Jaworski, J. M., Boucher, A., Yang, H., Slatina, T., & He, Z. (2018). Coded - Aperture Imaging with High - Resolution Large - Volume CZT. *2018 IEEE Nuclear Science Symposium and Medical Imaging Conference Proceedings (NSS/MIC)*, C, 1–5.
- Wang, J., & Zhao, Y. (2021). SNR of the coded aperture imaging system. *Optical Review*, 28(1), 106–112. <https://doi.org/10.1007/s10043-020-00639-z>
- Wang, L. (2017). Early diagnosis of breast cancer. *Sensors (Switzerland)*, 17(7). <https://doi.org/10.3390/s17071572>
- Weinstein SP, Slanetz PJ, L. A. (2021). Supplemental Breast Cancer Screening Based on Breast Density Variant. *ACR Appropriateness Criteria*, 1–17.
- Welcome to GATE's Documentation. (n.d.). Retrieved August 14, 2022, from <https://opengate.readthedocs.io/en/latest/index.html>
- Whiteley, W., Panin, V., Zhou, C., Cabello, J., Bharkhada, D., & Gregor, J. (2021). FastPET: Near Real-Time Reconstruction of PET Histo-Image Data Using a Neural Network. *IEEE Transactions on Radiation and Plasma Medical Sciences*, 5(1), 65–77. <https://doi.org/10.1109/TRPMS.2020.3028364>
- Wiebe, L. I. (1984). Radionuclides, radiotracers and radiopharmaceuticals for in vivo diagnosis. *Radiation Physics and Chemistry*, 24(3–4), 365–372. [https://doi.org/10.1016/0146-5724\(84\)90073-6](https://doi.org/10.1016/0146-5724(84)90073-6)
- XIANLING, D. (2017). ADAPTIVE BUTTERWORTH SINOGRAM FILTER FOR Tc-99m BREAST SPECT IMAGING WITH WIRE MESH COLLIMATOR. *PhD Thesis, Universiti Putra Malaysia, Malaysia*.
- Yaffe, M. J., & Mainprize, J. G. (2011). Risk of radiation-induced breast cancer from mammographic screening. *Radiology*, 258(1), 98–105. <https://doi.org/10.1148/radiol.10100655>
- Zaidi, H. (1999). Relevance of accurate Monte Carlo modeling in nuclear medical imaging. *Medical Physics*, 26(4), 574–608. <https://doi.org/10.1118/1.598559>
- Zeng, G. L. (2001). Image reconstruction - A tutorial. *Computerized Medical Imaging and Graphics*, 25(2), 97–103. [https://doi.org/10.1016/S0895-6111\(00\)00059-8](https://doi.org/10.1016/S0895-6111(00)00059-8)

- Zeniya, T., Watabe, H., Aoi, T., Kim, K. M., Teramoto, N., Hayashi, T., Sohlberg, A., Kudo, H., & Iida, H. (2004). A new reconstruction strategy for image improvement in pinhole SPECT. *European Journal of Nuclear Medicine and Molecular Imaging*, 31(8), 1166–1172. <https://doi.org/10.1007/s00259-004-1510-4>
- Zhang, A., Li, P., Liu, Q., & Song, S. (2017). Breast-specific gamma camera imaging with ^{99m}Tc-MIBI has better diagnostic performance than magnetic resonance imaging in breast cancer patients: A meta-analysis. *Hellenic Journal of Nuclear Medicine*, 20(1), 26–35. <https://doi.org/10.1967/s002449910503>
- Zhang, R., Tang, X., Gong, P., Wang, P., Zhou, C., Zhu, X., Liang, D., & Wang, Z. (2020). Low-noise reconstruction method for coded-aperture gamma camera based on multi-layer perceptron. *Nuclear Engineering and Technology*, 52(10), 2250–2261. <https://doi.org/10.1016/j.net.2020.03.024>
- Ziessman, H. A., O'Malley, J. P., & Thrall, J. H. (2006). Nuclear Medicine, The Requisites. In *Clinical Nuclear Medicine* (Vol. 20, Issue 6). <https://doi.org/10.1097/00003072-199506000-00032>